



Review

Electromechanical Nanogenerators for Cell Modulation

Zhirong Liu^{1,2,†}, Zhuo Wang^{1,2,†} and Linlin Li^{1,2,*}

¹ Beijing Institute of Nanoenergy and Nanosystems, Chinese Academy of Sciences, Beijing 101400, China; liuzhirong@binn.cas.cn (Z.L.); wangzhuo@binn.cas.cn (Z.W.)

² School of Nanoscience and Technology, University of Chinese Academy of Sciences, Beijing 100049, China

* Correspondence: lilinlin@binn.cas.cn

† These authors contribute equally to this work.

Abstract: Bioelectricity is an indispensable part of organisms and plays a vital role in cell modulation and tissue/organ development. The development of convenient and bio-safe electrical stimulation equipment to simulate endogenous bioelectricity for cell function modulation is of great significance for its clinical transformation. In this review, we introduce the advantages of an electromechanical nanogenerator (EMNG) as a source of electrical stimulation in the biomedical field and systematically overview recent advances in EMNGs for cell modulation, mainly including cell adhesion, migration, proliferation and differentiation. Finally, we emphasize the significance of self-powered and biomimetic electrostimulation in cell modulation and discuss its challenges and future prospects in both basic research and clinical translation.

Keywords: triboelectric nanogenerator; piezoelectric nanogenerator; electromechanical conversion; self-powered; cell modulation



Citation: Liu, Z.; Wang, Z.; Li, L. Electromechanical Nanogenerators for Cell Modulation. *Nanoenergy Adv.* **2022**, *2*, 110–132. <https://doi.org/10.3390/nanoenergyadv2010005>

Academic Editors: Ya Yang and Zhong Lin Wang

Received: 27 December 2021

Accepted: 3 March 2022

Published: 7 March 2022

Publisher's Note: MDPI stays neutral with regard to jurisdictional claims in published maps and institutional affiliations.



Copyright: © 2022 by the authors. Licensee MDPI, Basel, Switzerland. This article is an open access article distributed under the terms and conditions of the Creative Commons Attribution (CC BY) license (<https://creativecommons.org/licenses/by/4.0/>).

1. Introduction

Bioelectricity acting as an endogenous biophysical factor can modulate a myriad of cell behaviors, such as cell cycle, adhesion, proliferation, migration and differentiation, and further regulate important biological processes, such as embryogenesis and tissue regeneration [1–3]. Enlightened by endogenous bioelectricity, biomimetic electrical stimulation has been widely employed to regulate cell activities and offers widespread application potential for biomedical therapeutics [4]. At the same time, a series of electrical stimulation devices have been developed for in vitro and in vivo cell electrostimulation [5]. The commercial electrical stimulator is the most widely used device in basic biomedical research because its electrical parameters can be finely tuned from a wide range [6]. However, its bulky size brings a lot of inconvenience and causes poor patient compliance for clinical applications. Additionally, the long-distance wire connection between the stimulator and the target may increase potential safety risks. As another kind of commonly used electrical stimulator, the implantable battery is small and safe enough for in vivo applications; however, due to the limited battery capacity, regular battery replacement is required for long-term electrostimulation, which is expensive and increases the risk of postoperative infection [7].

To meet the requirements of small size, safety and long-term electrical stimulation at the same time, various new types of energy harvesters have been developed, which can collect energy from the surrounding environment or organisms and convert it into electricity [5]. Depending on the energy source, energy harvesters can be divided into three types: (i) environmental energy harvesters, including photovoltaic cells and pyroelectric nanogenerators [8]; (ii) mechanical energy harvesters, including triboelectric nanogenerators (TENG), piezoelectric nanogenerators (PENG) and electromagnetic generator (EMG) [1]; (iii) biochemical energy harvesters, including biofuel cells and non-pulley potential collectors [9,10]. Among them, several kinds of electromechanical nanogenerators (EMNGs) have drawn extensive attention in biomedical fields due to the existence of

abundant mechanical energy in organisms from tissue to cell level, such as cell activities, heartbeat, limb movement and respiration. An EMG is a kind of efficient, well-established and versatile mechanical energy harvester, and some high-frequency EMGs have been reported for *in vitro* cell electroporation [11–13]. However, an EMG only has superior performance at high frequencies and high dimensions [14], so they are less efficient in collecting low-frequency, disordered and weak mechanical energy in living organisms. Therefore, this review mainly focuses on recent advances in TENGs and PENGs for cell modulation (Figure 1). For a TENG, its basic working modes and its working mechanism are introduced. For a PENG, the methods used to generate a surface piezopotential for cell electrostimulation are discussed, including speaker, ultrasonic wave, magnetic field and cell/tissue activities. Then, the applications of EMNGs on cell modulation are elucidated, including cell proliferation, adhesion, migration, differentiation, etc. Finally, we discuss the challenges and scope for development of EMNGs for cell modulation in the future.

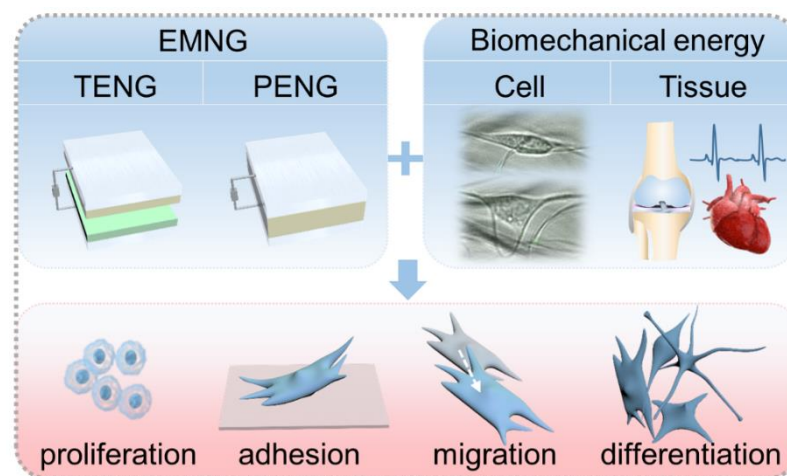


Figure 1. EMNGs driven by biomechanical energy for cell modulation, including cell proliferation, adhesion, migration and differentiation.

2. TENGs for Cell Modulation

2.1. Working Mechanism of TENGs

TENGs can collect abundant biomechanical energy from human bodies and convert it into electricity due to the coupling effect of triboelectrification and electrostatic induction [15–18]. Since its invention in 2012, the TENG mainly presents four basic operating modes, including the vertical contact–separation mode, lateral sliding mode, single electrode mode and freestanding triboelectric layer mode [19] (Figure 2a). Therefore, the structure of a TENG can be flexibly designed according to various applications. As their working principles are similar, herein the contact–separation mode is taken as an example to explain its working principle in detail (Figure 2b). Two films with different triboelectric properties are placed face to face as the friction layers and then metal is attached to their back as the electrode layer. In the original state, there is no induced charge (Figure 2b(i)). When the two friction layers are in contact with each other, an equal amount of opposite triboelectric charge is generated on the contact surface due to the triboelectric effect (Figure 2b(ii)). When the two friction layers are separated, it generates a potential difference between the two electrodes due to electrostatic induction. Thus, the electrons flow from the top electrode to the bottom electrode through the external circuit, thereby generating instantaneous current (Figure 2b(iii)), and then finally, it reaches equilibrium when the two friction layers are completely separated (Figure 2b(iv)). When the two friction layers make contact again, the induced charges flow back through the external circuit to compensate for the potential difference (Figure 2b(v)). The two friction layers continue to make contact and separate in order to generate an alternating current [20,21]. Due to the widespread existence of triboelectricity, TENGs have a wide range of material choices, from natural to

synthetic materials, which can meet the requirements for biocompatibility and flexibility in biomedical applications [22–24]. The combinations of friction layer materials that are commonly used in biomedical TENG can be divided into metal–polymer and polymer–polymer combinations [25]. For biomedical applications, especially implantable medical devices, it is necessary to select materials with good biocompatibility, low toxicity and potential biodegradability. Therefore, noble metals (Au, Ag and Pt) and transition metals (Mg, Fe and Zn) are selected as the metal friction or electrode layers. Polytetrafluoroethylene (PTFE), polyethylene terephthalate (PET), polyimide (Kapton), polydimethylsiloxane (PDMS) and polypropylene are common polymer friction layers for TENGs. Specifically, conductive polymers, such as polypyrrole (PPy), poly(3,4-ethylenedioxythiophene) (PEDOT), polythiophene (PTh) and polyaniline (PANI), can act as both polymer friction layers and electrodes. In the process of the contact and separation of two friction layers, their ability to gain and lose electrons depends on the triboelectric properties of the friction layer materials. According to the triboelectric sequence of common friction materials [26,27], the farther the distance between the two materials in the list, the greater the amount of charge transfer during the contact–separation process. In addition, the surface micro–nano structure, chemical modification or electron injection of the friction layer materials can increase its effective contact area and surface charge density, thus greatly improving the output performance of the TENG [28–30]. To meet the needs of short-term electrostimulation and avoid secondary surgery, biodegradable and bioabsorbable TENGs have also been designed using biodegradable or photothermal-tuned degradable materials [31–33], such as Mg, poly (caprolactone) (PCL), polylactic acid (PLA), poly(lactic-co-glycolide acid) (PLGA), poly (vinyl alcohol) (PVA), chitosan, cellulose, chitin and silk fibroin.

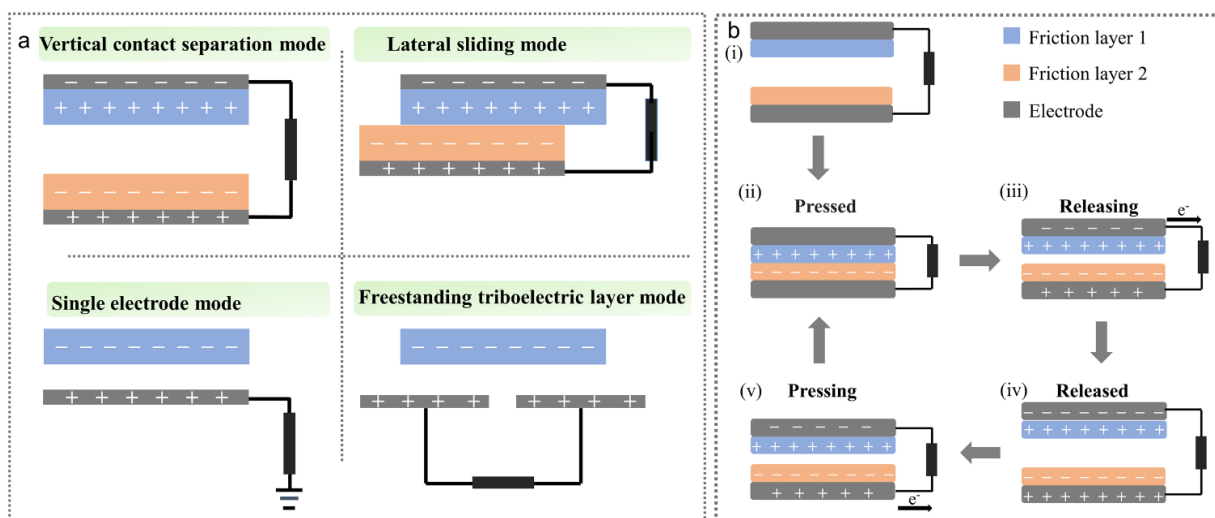


Figure 2. (a) The four fundamental working modes of a TENG: vertical contact–separation mode; lateral sliding mode; single electrode mode; and freestanding triboelectric layer mode. (b) The working principle of the TENG in contact–separation mode.

2.2. TENGs for Cell Modulation

Due to the above advantages, the TENG has developed rapidly in biomedical applications. Early research mainly focused on biomechanical energy harvesting, self-powered health monitoring and tissue-level electrical stimulation [22,34]. Recently, TENG-based electrostimulation has been used for cell modulation, mainly for promoting neural/osteogenic differentiation and directing cell migration and proliferation for wound healing.

2.2.1. TENGs for Nerve Repair

Neurons are electrical excitable cells from neural tissues, amongst others. It has been proven that electrostimulation can improve the synaptic function of neurons, thereby

promoting nerve regeneration and functional recovery [2]. For this application, a biodegradable TENG was designed that can be implanted into an animal for the electrical stimulation of nerve cells and gradually degrade after finishing its work [31]. The employed TENG has a multilayered structure, including the friction layers, the electrode layers and the encapsulation structure. Two biodegradable polymers are assembled together as the friction layers, and there is a 200 nm spacer layer between the two friction layers. The electrode layer is prepared by depositing a 50 nm magnesium (Mg) film on the back of the friction layer. The fabricated TENG is then encapsulated to improve its stability in the surrounding physiological environment. When applying this TENG to stimulate cells seeded on complementary micrograting electrodes (10 V/mm, 1 Hz), the nerve cell growth can achieve directional growth, which is of great significance for neural repair. Guo et al. combined a wearable TENG and electroconductive microfibers to construct a self-powered electrostimulation system for the neural differentiation of stem cells (Figure 3a,b) [35]. The prepared TENG worked based on the continuous contact and separation of the upper aluminum (Al) electrode and the bottom Kapton film attached to a copper (Cu) electrode. A 3 M foam (2 mm) was bound between the poly(methyl methacrylate) (PMMA) substrate and the upper electrode as a stress buffer layer to increase its output stability. The output of the TENG could reach about 300 V and 30 μ A when triggered by human walking (Figure 3c). The electroconductive microfibers were composed of poly(3,4-ethylenedioxythiophene) (PEDOT) and reduced graphene oxide (rGO), which can enhance the proliferation ability of mesenchymal stem cells (MSCs) and show a good neural differentiation tendency. Importantly, after 21 days of the continuous stimulation of the stem cells grown on the conductive hybrid microfibers by the TENG, the gene and protein expressions of both Tuj-1 (neuron-specific maker) and GFAP (neuroglia-specific maker) were significantly higher than those without electrical stimulation (Figure 3d,e). This work confirmed the feasibility and potential of TENGs in the field of neural differentiation and repair.

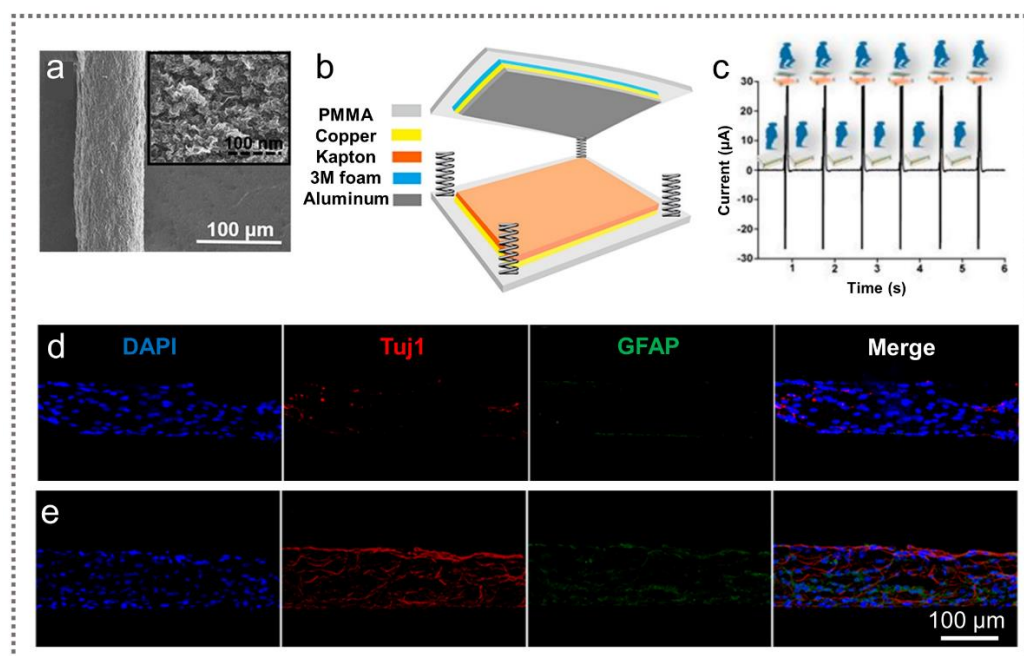


Figure 3. TENGs for nerve repair: (a) the micromorphology of the rGO–PEDOT microfiber; (b) the structural design of the TENG; (c) the output current of the TENG driven by normal human walking. The nucleus (blue), neuron-specific maker Tuj1 (red) and neuroglia-specific maker GFAP (green) of the cells (d) without electrostimulation and (e) with TENG-induced electrostimulation for 21 days. Reprinted with permission from ref. [35], Copyright 2016, American Chemical Society.

2.2.2. TENG for Bone Repair

Bone is a natural composite of piezoelectric materials, which mainly comprises a piezoelectric collagen matrix and hydroxyapatite crystals [36]. In the process of bone repair and regeneration, the electric signal is a vital factor for promoting the osteodifferentiation of stem cells and osteoblast proliferation [37,38]. Due to the abundant mechanical energy during joint movement, TENGs can effectively collect this energy and then convert it into electricity for bone repair. It has been confirmed that the electrostimulation of TENGs can promote osteoblast attachment, proliferation and differentiation. For example, Tian et al. developed a self-powered electrical stimulator for bone repair, consisting of an implantable TENG as the power source, a rectifier and an interdental electrode [39]. When the flexible TENG was implanted on the SD rat's femur, it could successfully convert the biomechanical energy of the rat's daily exercise into electricity. Applying the electricity generated by the TENG to the cells through the interdental electrode could effectively promote cell adhesion, spreading and proliferation. Moreover, the osteogenic differentiation level of the cells increased by 28.2% after stimulation for 12 days. Shi et al. utilized a TENG to load and accumulate negative charges on the surface of an anodized titanium implant for promoting the osteogenesis of MC3T3-E1 preosteoblast cells [40]. The prepared TENG worked based on the vertical contact–separation mode (Figure 4a). A PTFE film with a nanorod structure and a titanium (Ti) foil with a nanotube structure were used as the triboelectric layers. A thin copper (Cu) film was magnetron sputtered on the outer face of the PTFE friction layer as an electrode and a Ti foil was employed as another electrode. Then, PTFE tape and PDMS were used to encapsulate the TENG for waterproofing. The output of the TENG could reach up to 12 V, 0.15 μ A and 5.3 nC (Figure 4b) and its output voltage could be well maintained after 1×10^6 cycles. The prepared TENG could convert the biomechanical energy of human daily movement into electricity for constructing a long-term and stable negatively charged implant surface, thereby inhibiting bacterial adhesion and biofilm formation. Moreover, the negatively charged implant could promote preosteoblast adhesion and the osteogenic differentiation of MC3T3-E1 cells (Figure 4c). Yao et al. designed an implantable and bioresorbable TENG that could be attached to living tissue and generate bidirectional electric pulses (Figure 4d) [41]. An island–bridge magnesium (Mg) layer served as both the bottom electrode and a triboelectric layer. PLGA with a micropyramid structure was used as another triboelectric layer and the Mg electrode with the island–bridge structure was coated on the top of the PLGA layer, serving as the top electrode. The micropyramid structure of the PLGA could improve the output of the TENG due to the increase in contact area. The serpentine geometry and island–bridge structure of the electrode layer could effectively improve the robustness of the structure and reduce the modulus of the flexible device. Thus, it could be pasted to irregular tissues and withstand large strains. When applying the electrostimulation on a pair of dressing electrodes, the generated electric field could activate relevant growth factors (Figure 4e,f). The enhanced secretion of the fibroblast growth factor (FGF1) and vascular endothelial growth factor (VEGF) could accelerate vascularization for nutrient supply and metabolic transportation. More transforming growth factor and bone morphogenetic protein could promote cell differentiation and accelerate bone formation and mineralization (Figure 4g). In general, the electrostimulation through the TENG could regulate the bone microenvironment, promote rapid bone regeneration and synergistically increase bone strength and mineral density (Figure 4h).

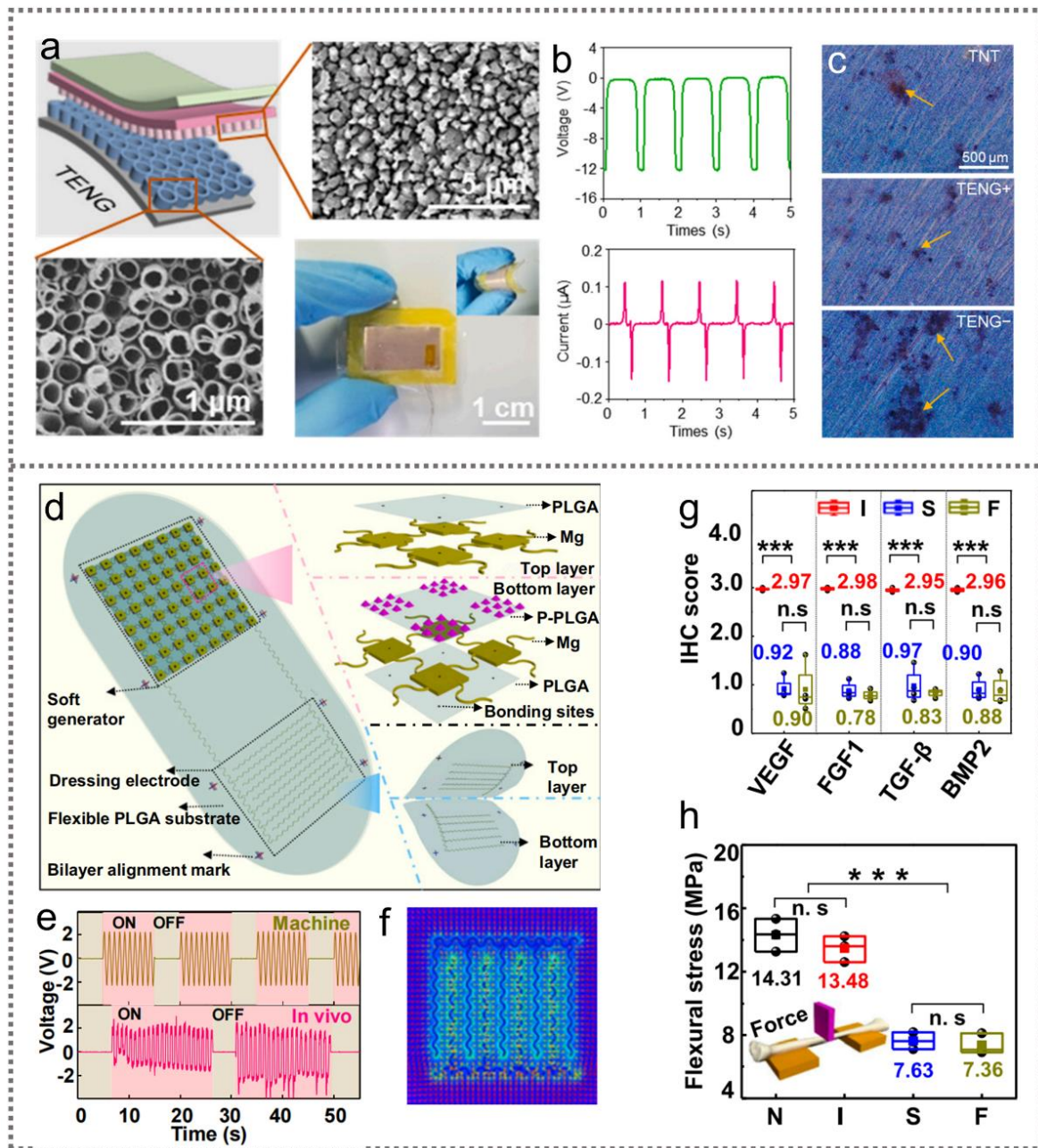


Figure 4. TENGs for bone repair: (a) the surface microstructure and photograph of the prepared TENG; (b) the output voltage and current of the TENG; (c) alizarin red staining showing the calcium deposits of MC3T3-E1 after TENG electrostimulation for 21 days. Reprinted with permission from ref. [40], Copyright 2020, Elsevier. (d) The schematics of the implantable self-powered bone fracture electrostimulation device, consisting of a TENG as a power source and a pair of dressing electrodes for applying electrostimulations to the fracture; (e) the output voltage of the TENG driven by a mechanical linear motor (top) and on a rat (bottom); (f) the simulated electrical field distribution of the dressing electrodes inside a tissue under the voltage of 4 V; (g) the immunohistochemistry (IHC) score of the expressed growth factors in different groups; (h) the three-point bending flexural stress measurement for the different groups after 6 weeks. N, normal group; I, dressing electrodes with TENG electrostimulation; S, dressing electrodes without TENG electrostimulation; F, no implanted device. n.s. and *** represent non-significant and $p < 0.001$, respectively. Reprinted with permission from ref. [41], Copyright 2021, the Authors. Published by PNAS.

2.2.3. TENGs for Wound Healing

In addition, the endogenous electric field also plays key roles in wound healing. Generally, skin wounds have a transepithelial potential of 15–60 mV, which serves as a directional cue to direct cell proliferation and migration to the wound site for wound healing [42]. Thus, electrostimulation is an attractive auxiliary method for wound repair (Figure 5a). However, it is still largely limited in clinical applications due to the inconvenience of its implementation. To solve this problem, a wearable electrostimulation bandage was designed to accelerate the healing of skin wounds [43,44]. It was composed of a wearable TENG as a power supply and a pair of dressing electrodes, both of which were integrated in a bandage [43]. The TENG was prepared by overlapping a Cu (electropositive material) electrode layer with a Cu/PTFE (electronegative material) film on the PET substrate. After wrapping the bandage on the chest of the rat, the TENG could collect the mechanical energy of the rat's breathing to generate electricity. When the rat was under deep anesthesia, the output voltage was only ~0.2 V at a rate of 30 times per min, which corresponded to a slow and shallow breathing pattern. After the rat recovered from anesthesia, the output voltage reached ~1.3 V at a rate of 40 times per min, corresponding to the calm and stable state of the rat. When the rat moved normally, the output voltage reached the highest level of ~2.2 V at a rate of 110 times per min (Figure 5b). Under the electric field induced by the TENG (2 V cm^{-1} , 1 Hz), fibroblasts exhibited an obvious proliferation and alignment. After 6 h of the electric field stimulation, cells continued to proliferate and differentiate along the direction of the electric field (Figure 5c). Fibroblasts play a crucial role in the healing process of skin wounds. Initially, cells migrate to the wound, proliferate and interact with surrounding cells. After that, fibroblasts differentiate and generate ECM, glycoproteins, adhesive molecules and various cytokines, which then replace the provisional fibrin-based matrix and accelerate wound repair. Under the treatment of the electrostimulation bandage, a full-thickness rectangular skin wound was quickly closed within 3 days, while the normal shrinkage-based healing process needs 12 days. Li et al. also confirmed the promoting effect of TENG electrostimulation on tissue repair. Their prepared TENG was implantable and its degradation rate could be tuned in vivo by near-infrared (NIR) light irradiation [33]. The biodegradable TENG consisted of three parts: an Au deposited, hemisphere array-structured layer served as both the triboelectric layer and the bottom electrode; a biodegradable polymer was another triboelectric layer; and a thin Mg film was deposited on the back as the top electrode. Another biodegradable polymer doped with Au nanorods (AuNRs) was applied as the bottom substrate, which endowed the TENG's ability to respond to NIR irradiation so that the biodegradation process could be rationally controlled (Figure 5d). The open-circuit voltage (V_{oc}) and short-circuit current (I_{sc}) of the TENG reached 28 V and 220 nA, respectively. After implantation in the subdermal region on the back of the SD rats, the V_{oc} was about 2 V. With NIR treatment, the output of the TENG quickly dropped to 0 within 24 h and the device was largely degraded in 14 days (Figure 5e,f). Applying the output of the TENG to stimulate fibroblasts (100 mV mm^{-1}) could significantly accelerate the migration of cells across the scratch, which was essential for the wound healing treatment (Figure 5g,h).

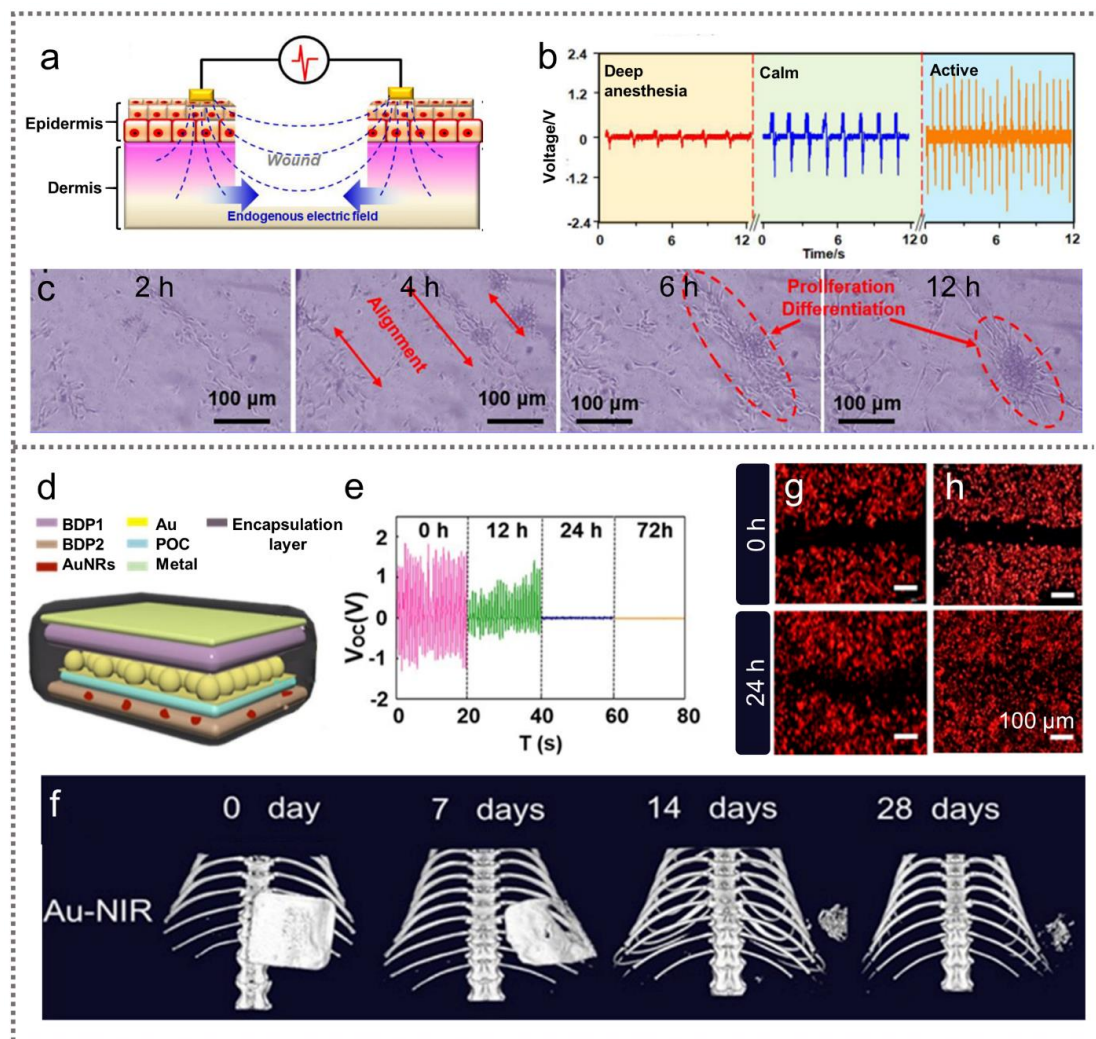


Figure 5. TENGs for wound healing: (a) the mechanism of wound healing under the endogenous electric field; (b) the output voltage of the TENG driven by different frequencies of breathing in rats; (c) the morphology of the NIH 3T3 cells after TENG electrical stimulation of different times. Reprinted with permission from ref. [43], Copyright 2018, American Chemical Society. (d) The structure design of the photothermal-controlled biodegradable TENG; (e) the output of the TENG with NIR irradiation; (f) a micro-CT image of the implanted TENGs over time. Fluorescence microscope images of fibroblast L929 cell migration (g) without electrostimulation and (h) with TENG electrostimulation. Reprinted with permission from ref. [33], Copyright 2018, Elsevier.

2.2.4. TENGs for Drug Delivery and Cardiac Pacing

In addition to the aforementioned applications, TENGs have also been employed to construct self-powered electroporation systems to improve the permeability of cell membranes for drug delivery or drug release. Electroporation utilizes high-intensity electric fields to create transient nanopores in plasma membranes to introduce biomolecules into cells. Liu et al. integrated a TENG with a silicon nanoneedle array electrode to build a self-powered nanoelectroporation system for facilitating efficient intracellular drug delivery while minimizing cellular damage (Figure 6a) [45]. In this system, the TENG acted as a self-powered and stable electrostimulation source to provide electrical pulses for electroporation, which made the system more convenient in practical applications. On the other hand, a silicon nanoneedle array was employed to replace the traditional planar electrode for nanoelectroporation, which could only generate high local electrical fields in the nanoneedle-adherent cell interface, thereby reducing cell damage (Figure 6b). This system could deliver a variety of exogenous species, such as small molecules, siRNA and biomacromolecules,

into different types of cells. Depending on the delivered biomolecule and cell type, the delivery efficiency ranged from 50% to 90% and cell viability was above 94% (Figure 6c). On this basis, the same group further designed a high-throughput electroporation system based on a TENG and silver nanowire-modified foam electrodes [28]. Cell suspension could continuously flow through the foam electrodes in the electroporation channel to achieve electroporation under the action of the TENG's electrical pulses (Figure 6d). The system could achieve high cell processing throughput of up to 10^5 cells/min while ensuring high cell delivery efficiency and viability. Yang et al. also designed a self-powered gene electrotransfection system that consisted of a TENG and a nanowire array electrode [46]. The employed TENG was based on the vertical contact–separation mode, which could harvest the mechanical energy of the simple human tapping motion and convert it into electricity for electrotransfection. Two CuO nanowire array meshes were coaxially placed as electrodes, which could greatly amplify the local electric field strength to enhance the transfection efficiency and reduce cell damage. The system could achieve a high-efficiency siRNA electrotransfection of 95% for MiaPaCa-2 cells and 84% for K562 cells, and then downregulate the expression of targeted mutation genes, thereby significantly inhibiting cell proliferation and anti-apoptosis ability. Zhao et al. loaded doxorubicin (DOX) into red blood cells (D@RBC), which could create transient pores in the cytomembrane through TENG electroporation and release DOX on demand to kill tumor cells for cancer therapy (Figure 6e–g) [47]. These results illustrate that TENG-based self-powered systems have great potential for both fundamental biological research and clinical applications.

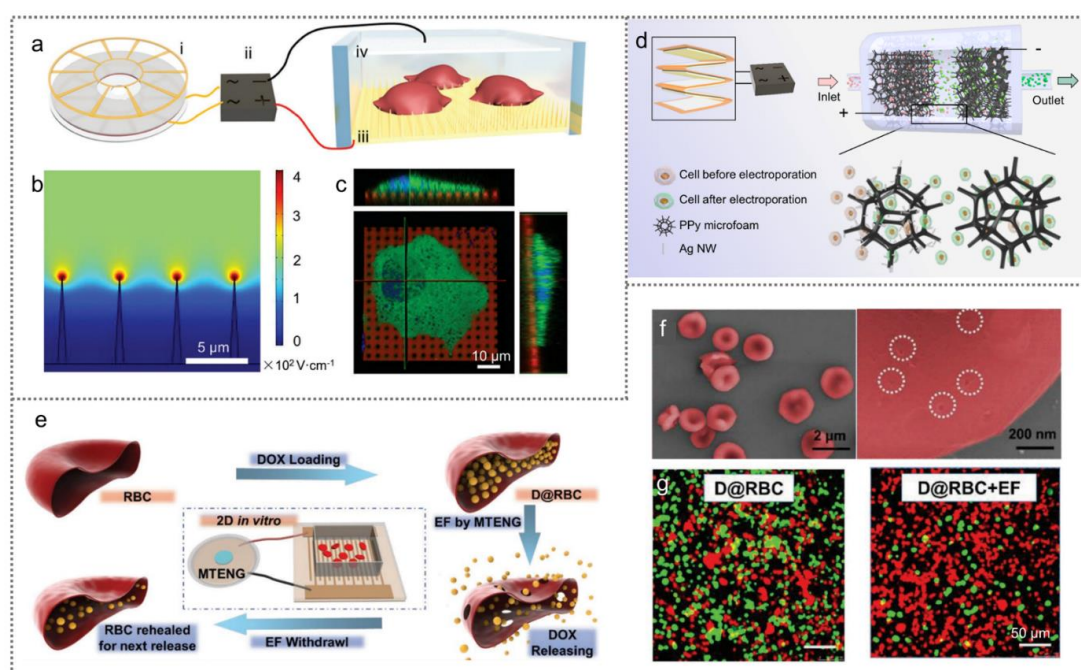


Figure 6. TENGs for drug delivery: (a) a schematic illustration of the TENG-driven electroporation system based on a nanoneedle array electrode; (b) the simulated electrical field distribution of the nanoneedle array with an applied voltage of 20 V; (c) a fluorescence image of MCF-7 after delivering dextran-FITC (green). Reprinted with permission from ref. [45], Copyright 2019, WILEY-VCH. (d) A schematic illustration of the TENG-driven high-throughput electroporation system. Reprinted with permission from ref. [28], Copyright 2020, American Chemical Society. (e) A schematic illustration to show the controlled release of DOX from RBC driven by the TENG; (f) SEM images of D@RBC under the electric field; (g) the viabilities of HeLa cells in the D@RBC and D@RBC under the electric field groups (live cells are green and dead cells are red). Reprinted with permission from ref. [47], Copyright 2019, WILEY-VCH.

Cardiomyocytes are also electrically active cells and their action potentials contribute to the spontaneous beating of the cells. Rhythmic action potentials propagate continuously in multicellular cardiac tissue and travel through the myocardium to induce myocardial contraction [1]. Therefore, electrical stimulation has been used in heart failure treatments and myocardial reconstruction. Inspired by this, Ouyang et al. demonstrated a self-powered symbiotic pacemaker based on an implantable TENG [48]. The V_{OC} of the implantable TENG was as high as 65.2 V. The energy collected from each heartbeat was about 0.495 μ J, which was above the endocardial pacing threshold energy (0.377 μ J). Thus, this self-powered symbiotic pacemaker successfully corrected sinus arrhythmia and prevented disease progression on a large animal model.

3. PENGs for Cell Modulation

PENGs can convert mechanical motion into electric energy based on piezoelectric materials and piezoelectric effects. A PENG is composed of piezoelectric materials, positive and negative electrodes and flexible substrates. Among them, the piezoelectric material is the core component of a PENG and is the basis for generating electricity.

3.1. Piezoelectric Materials and Piezoelectricity

Piezoelectric material is a kind of dielectric material with a non-centrosymmetric structure, which can generate and accumulate charges with opposite signs on its surface under the action of mechanical stress or strain [49]. According to compositions, piezoelectric materials can be divided into three categories: (i) inorganic piezoelectric materials; (ii) organic piezoelectric materials; and (iii) composite piezoelectric materials.

Inorganic piezoelectric materials mainly include piezoelectric single crystals, piezoelectric ceramics and piezoelectric semiconductors. Quartz, lithium niobate, lithium gallate, lithium germanate and lithium tantalate are several common piezoelectric single crystals. Piezoelectric ceramics often have strong piezoelectricity and high dielectric constants, such as barium titanate ($BaTiO_3$), lead zirconate titanate (PZT), lead zinc niobium (PZN), lead metaniobate and lead barium lithium niobate. Generally, piezoelectric ceramics containing lead have high piezoelectric coefficients, but the toxicity of lead limits their application in the biomedical field. Currently, most piezoelectric semiconductors have wurtzite structures and have both piezoelectricity and semiconducting properties, such as ZnO, GaN, AlN and BN. The piezoelectricity of inorganic materials originates from the non-centrosymmetric crystal structure. Taking wurtzite-structured ZnO as an example (Figure 7a,b), positive Zn^{2+} and negative O^{2-} have tetrahedral coordination in an unstrained hexagonal ZnO crystal structure. So, the centers of the anions and cations overlap each other and there is no polarization. When the crystal is under a mechanical stress, the displacement of Zn^{2+} and O^{2-} inside the crystal causes the positive and negative charge centers to shift in opposite directions, resulting in a dipole moment in the unit cell [50]. Due to the continuous superposition of the dipole moments, a macroscopic piezoelectric potential (piezopotential) is generated in the ZnO crystal (Figure 6b) [51].

Compared to inorganic piezoelectric materials, although the piezoelectric properties of organic piezoelectric materials are relatively poor, their advantages of good biocompatibility, processability and high flexibility can satisfy the requirements for biomedical applications, especially for wearable and implantable devices. Organic piezoelectric materials can be divided into natural and synthetic piezopolymers. Collagen, chitosan, cellulose and chitin are widely studied natural piezoelectric polymers. PVDF and its trifluoroethylene (TrFE) copolymer (P(VDF-TrFE)), poly-L-lactic acid (PLLA) and polyhydroxyalkanoates (PHAs) are representative synthetic piezopolymers. The piezoelectricity in organic materials arises from their non-centrosymmetric molecular arrangement and orientation. Figure 6c depicts the piezoelectric effect of PVDF ($(CH_2-CF_2)_n$). PVDF has five crystal phases, in which α -phase with trans-gauche-trans-gauche conformation (TGTG') and a β -phase with all trans conformation (TTTT) are predominant [52,53]. The dielectric property of PVDF is caused by the difference in electronegativity between F and H atoms that leads to a

dipole moment is generated along the $F \rightarrow H$ direction [54]. For α -phase PVDF, there is no piezoelectricity since the chains are arranged in the unit cell, resulting in a net cancellation of the dipole moments. For β -phase PVDF, since the parallel orientation of the dipole moments leads to the overlay of the electric dipole moments, it has the highest piezoelectricity [55] (Figure 7c). Composite piezoelectric materials are often obtained by dispersing piezoelectric nanoceramics into a polymer matrix, which combines the advantages of inorganic piezoelectric materials and piezoelectric polymers, showing good flexibility, high piezoelectric coefficients and processability. Piezoelectric materials with high mechanical and piezoelectric properties are the basis for the fabrication of high-performance PENGs.

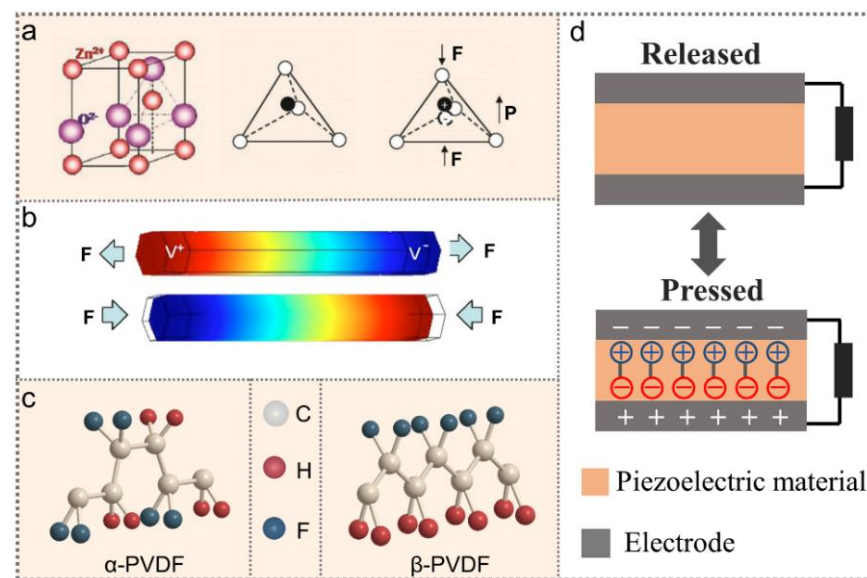


Figure 7. (a) An atomic model of a wurtzite structure ZnO and a schematic diagram of a stress-induced electric dipole moment. Reprinted with permission from ref. [50], Copyright 2012, WILEY-VCH. (b) Piezopotential distribution along a ZnO nanowire under axial stretch or compress. Reprinted with permission from ref. [51], Copyright 2009, American Institute of Physics. (c) The molecular structure of α -phase and β -phase PVDF; (d) the working principle of the PENG.

3.2. Working Mechanism of PENGs

In 2006, Wang et al. first developed a zinc oxide (ZnO) nanowire-based PENG to collect tiny vibrational energy [56]. In 2010, a PENG that was based on single ZnO nanowire was successfully implanted in a live rat to harvest mechanical energy from its breath and heartbeat, with an output of around 3 mV and 30 pA [57]. After that, all kinds of piezoelectric materials and structures have been applied to fabricate implantable PENGs, including PVDF, P(VDF-TrFE), ZnO nanowire arrays, PZT, etc. [58–64]. Traditionally, a PENG is composed of an intermediate piezoelectric layer and two metal electrodes in a sandwich structure. Figure 7d demonstrates the electrical generation principles of a typical PENG. At the beginning, without the action of external force, the charge centers of the anions and cations overlap each other, so there is no polarization in the piezoelectric material. When mechanical stress is applied, the piezoelectric material is compressed and deformed, so that the anions and cations inside the crystal are displaced and the positive and negative charge centers are separated to generate a surface piezopotential. The electrons flow through the external circuit to achieve charge balance, thereby generating piezoelectric current output. When the external force is removed, the piezopotential gradually decreases and disappears and the electrons flow back to rebalance the charge. During the cyclic compression–release process, mechanical energy is continuously converted into electrical energy [65,66]. The selection of piezoelectric materials that have excellent performance is the key to improving the output of PENGs. In addition, the crystallinity of piezoelectric

materials and the arrangement direction of dipoles can be further improved by means of annealing, stretching and high-voltage polarization, thereby achieving efficient mechanical energy harvesting [66].

3.3. PENGs for Cell Modulation

A PENG is an energy harvesting device that converts mechanical energy into electrical energy using the piezoelectric effect. Therefore, its application is similar to that of a TENG and it too can be used as a self-powered electrical stimulation source. For example, Zhang et al. proposed a biomechanical energy-driven shape-memory PENG for promoting MC3T3-E1 cell proliferation and orientation and osteogenic differentiation [67]. Jin et al. designed a tribo/piezoelectric hybrid nanogenerator to promote the long-term proliferation and migration of Schwann cells and regenerate the myelination of nerve fibers and neuromotor function reconstruction [68]. In addition to being an electrical stimulation source, some piezoelectric materials are also employed as biological scaffolds [54]. Therefore, piezoelectric biomaterials can be designed for in situ cell-scale electrical stimulation, avoiding wire connections and electrode implantation. External mechanical force or deformation is an essential precondition for piezoelectric biomaterials to generate piezoelectric potential (piezopotential) for cell electrostimulation. The methods commonly used to apply mechanical force are acoustic waves, magnetic fields and cell traction.

3.3.1. Acoustic Wave-Driven PENGs for Cell Modulation

An acoustic wave is a mechanical wave that is generated by the vibration of a sound source. Acoustic pressure, i.e., the pressure change caused by sound waves, is the main source of mechanical force. According to the frequency, acoustic waves can be divided into four categories: infrasound (<20 Hz); audible sound (20–20 kHz); ultrasound (20 kHz–1 GHz); and hypersound (>1 GHz). Wang et al. fabricated electrospun poly(vinylidene fluoride-trifluoroethylene) (P(VDF-TrFE)) nanofibers with a d_{31} of 16.17 pC/N [69]. A lab-designed speaker was employed to generate the mechanical vibration to deform the nanofibers. Under the dual effects of the nanofiber morphology and electrical stimulation (0.75 V, 22.5 nA), L929 fibroblast cells aligned perfectly along the direction of the nanofibers and the cell proliferation rate increased by 1.6-fold.

An ultrasonic wave is a commonly used mechanical force source in the field of biomedicine because of its high tissue penetration and good directionality [70] and its ultrasonic power, frequency and period can be adjusted precisely. In the ultrasonic process, acoustic pressure and ultrasonic cavitation effects play major roles in driving the deformation of piezoelectric materials [71]. When the sound pressure gradually reaches a certain value, the tiny bubble cores in the liquid expand rapidly and then suddenly close to generate the shock wave. The ultrasonic cavitation is a series of the dynamic processes, such as expansion, collapse and generation, of microjets. Wan et al. demonstrated an ultrasound-mediated cell sheet harvesting based on a piezoelectric polyvinylidene fluoride (PVDF)/barium titanate (BaTiO_3 , BTO) composite film (Figure 8a) [72]. Under the ultrasound stimulation (1 MHz, 0.8 W cm^{-2}), the output voltage and current of the PVDF/BTO film could reach ~100 mV and 0.19 nA, respectively. The adsorption and conformation of fibronectin (FN) play an important role in regulating early cell material adhesion. After ultrasound treatment for 20 s, the surface potential of the PVDF/BTO film was more negative, thereby decreasing the FN adsorption to manipulate cell adhesive behavior. On the other hand, the generated piezopotential under ultrasound stimulation could regulate the secondary structure of adhesive protein fibronectin (FN) from β -sheet to α -helix, thereby weakening the interfacial protein interaction and further regulating the cell adhesion behavior (Figure 8b,c). In addition, ultrasound assisted piezoelectric biomaterials have also been employed for inducing neural differentiation [73–76]. Marino et al. prepared piezoelectric tetragonal BTO nanoparticles that could be attached to the cell membrane [76]. Under ultrasound stimulation, the generated piezopotential activated voltage-gated membrane channels, allowed calcium and sodium to flow in and then mediated the enhancement of

neurite outgrowth. Liu et al. designed a biohybrid multifunctional micromotor composed of magnetic Fe_3O_4 nanoparticles, piezoelectric BTO nanoparticles and *S. platensis* [74]. The micromotor was actuated and steered magnetically using a low-intensity rotating magnetic field (Figure 8d,e). Due to its diameter ($\approx 0.8 \mu\text{m}$) being smaller than the size of neural stem-like cells, this micromotor could reach the desired position at the single cell level. After reaching the targeted neural stem-like cell, the in situ piezopotential of BTO was generated by an ultrasound stimulation, which activated the Ca^{2+} channels and thereby induced the neuronal differentiation of the targeted cells (Figure 8f,g). Additionally, piezoelectric nanoparticles can be endocytosed by the cells to achieve non-destructive intracellular electrical stimulation for promoting osteogenic differentiation. Ma et al. synthesized piezoelectric nylon-11 nanoparticles with uniform morphology that could be easily endocytosed using dental pulp stem cells (DPSCs) [77]. Under ultrasound conditions, piezoelectric stimulation generated by nylon-11 nanoparticles could efficiently promote the osteogenic differentiation of stem cells through electromechanical conversion in a non-invasive way. Ultrasound assisted piezoelectric biomaterials can also regulate proinflammatory macrophage polarization [78], which is critical for antitumor immunity. After ultrasound treatment on β -PVDF, a significant upregulation of the mRNA levels of proinflammatory (M1) markers was observed, including $\text{TNF-}\alpha$, $\text{IL-1}\beta$ and MCP-1 (Figure 8h–j). In addition, the intensity of intracellular M1 marker iNOS was higher than that on tissue culture plates (TCPs), while anti-inflammatory (M2) marker Arg-1 was significantly reduced (Figure 8k,l). These results prove that the piezoelectricity of β -PVDF obviously promotes M1 polarization.

3.3.2. Magnetic Field-Driven PENGs for Cell Modulation

Magnetic fields have also been employed to induce piezopotential by rationally designing magneto-electric (ME) composite materials. ME materials comprise a class of multifunctional nanostructures that are capable of strongly coupling magnetic and electric fields. The ME effect is defined as the electrical polarization of a substance in response to a magnetic field (positive effect) or the magnetization change of a substance under the action of an electric field (converse effect) [79]. ME materials include single phase and composite materials, within which the composites that are composed of a ferromagnetic phase and a piezoelectric phase have larger ME effects at room temperature [80]. Under the action of the magnetic field, the magnetic material is deformed and the strain is further transferred to the closely connected piezoelectric material to generate piezopotential. This phenomenon is the magneto-electric coupling in two-phase ME materials. The properties of ME composite materials can be regulated by changing the phase materials, component sizes and phase volume ratios [81]. Core shell-structured ME materials have attracted considerable attention in the design of drug delivery systems, which are capable of controlling drug release via external magnetic fields. For example, Nair et al. designed $\text{CoFe}_2\text{O}_4@ \text{BaTiO}_3$ ME nanoparticles that could generate piezopotential by applying a low alternating current magnetic field to allow controlled on-demand drug release [82]. The application of ME composites for the electrical stimulation of cells and tissues has been intensively studied in tissue engineering. Mushtaq et al. designed a soft hybrid nanorobot that mimicked an electric eel, based on the magneto-electric coupling effect [83]. These bionic nanoeels consisted of three parts: a flexible and elongated piezoelectric PVDF tail connected to a polypyrrole nanowire, which was decorated with nickel rings for magnetic actuation (Figure 9a). Upon the rotating magnetic fields, the nanoeels displayed different swimming modes, including tumbling, wobbling and corkscrewing (Figure 9b). At the same time, the piezoelectric soft tail was driven to deform, causing its electric polarization. As magnetic fields can achieve deep tissue penetration and can control the movement of magnetic materials with high precision, they can be used to achieve targeted local electrical stimulation. Dong et al. introduced a highly integrated multifunctional soft helical microswimmer based on $\text{CoFe}_2\text{O}_4@ \text{BiFeO}_3$ (CFO@BFO) core shell ME nanoparticles, which could realize targeted neuronal cell delivery, on-demand localized neuron electrostimulation and post-delivery enzymatic degradation (Figure 9c) [84]. Under a rotating magnetic field, the

helical microswimmer rotated around its long axis and moved in translation (Figure 9d). After reaching the target position, an alternating magnetic field was applied to induce the magnetostriction of the CFO core and then the pressure was transferred to the BFO shell to generate piezopotential, thus promoting the neuronal differentiation of the cells (Figure 9e–g). The prepared microswimmer could be degraded by the enzymes in the ECM produced by the cells. Fang et al. prepared a stretchable carbon porous nanocookies@conduit (NC@C) using 3D printing technology, in which the NC was composed of rGO, mesoporous silica and carbon layers with an excellent magneto-electric effect. The prepared NC@C could encapsulate the neuron growth factor (NGF) and achieve on-demand release under the control of a magnetic field. At the same time, it could electrically stimulate cells to effectively induce cell proliferation and neuronal differentiation in vitro and could further improve myelin layers and guide axonal orientation in vivo (Figure 9h–j) [85]. In addition, ME materials have also been developed for deep brain stimulation, bone regeneration, skeletal muscle tissue regeneration and more [85–88]. These materials inspire new approaches to targeted cell therapies for traumatic injuries.

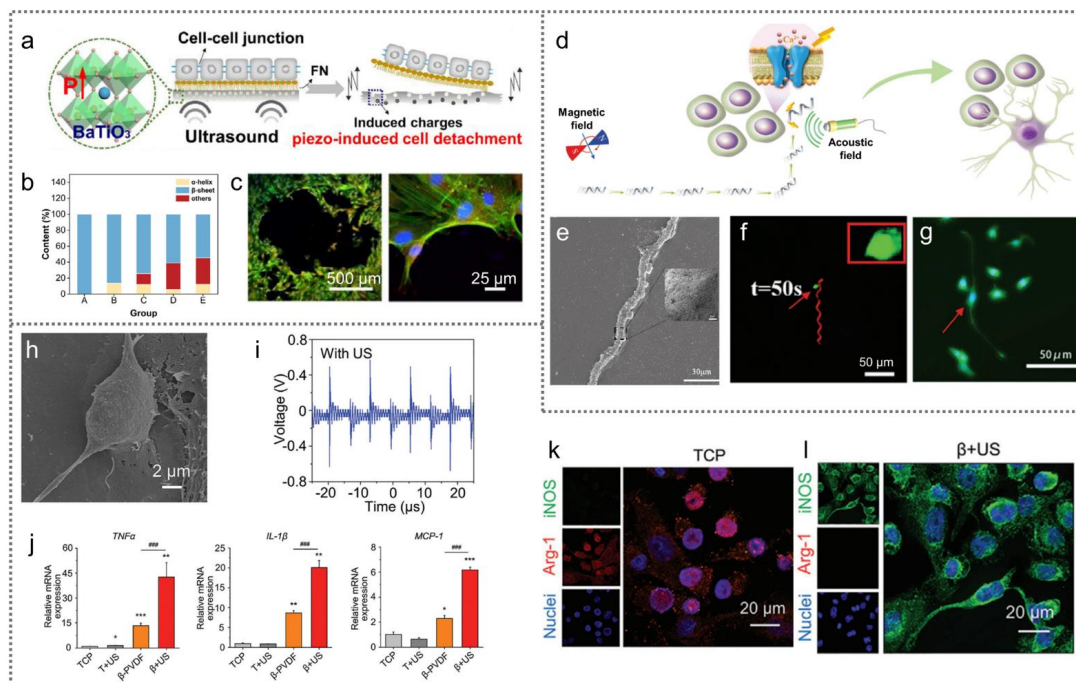


Figure 8. Ultrasound-driven PENGs for cell modulation: (a) a schematic diagram of the cell detachment regulated by piezopotential; (b) the contents of fibronectin α -helix and β -sheet under different conditions (A, FN in PBS; B, FN on the PVDF/BTO film; C, FN under ultrasound; D, E, FN on the PVDF/BTO film under ultrasound); (c) fluorescence microscopy images of cells remaining on the PVDF/BTO composite film after ultrasound. Reprinted with permission from ref. [72], Copyright 2021, Elsevier. (d) An illustration of a highly controllable micromotor for inducing the neuronal differentiation of targeted cells; (e) SEM images of *S.platensis*@Fe₃O₄@tBaTiO₃; (f) representative time-lapse Ca²⁺ imaging of PC12 cell stimulated by *S.platensis*@Fe₃O₄@tBaTiO₃ with ultrasound; (g) a fluorescent image of differentiated PC12 cells stimulated by *S.platensis*@Fe₃O₄@tBaTiO₃ with ultrasound (targeted cell indicated with a red arrow). β III-tubulin is stained in green and the nuclei are in blue. Reprinted with permission from ref. [74], Copyright 2020, WILEY-VCH. (h) A representative SEM image of THP-1 cells on β -PVDF for 24 h; (i) the output voltage of β -PVDF with ultrasound stimulation; (j) the relative mRNA expression of the M1 markers of TNF- α , IL-1 β and MCP-1 in different groups; (k,l) immunofluorescence staining images of M1 marker iNOS and M2 marker Arg-1 after culturing for 3 days on TCP and β -PVDF with ultrasound. * $p < 0.05$, ** $p < 0.01$, *** $p < 0.001$ vs. the TCP control group, ### $p < 0.001$ vs. the β -PVDF group. Reprinted with permission from ref. [78], Copyright 2021, The Authors. Published by WILEY-VCH.

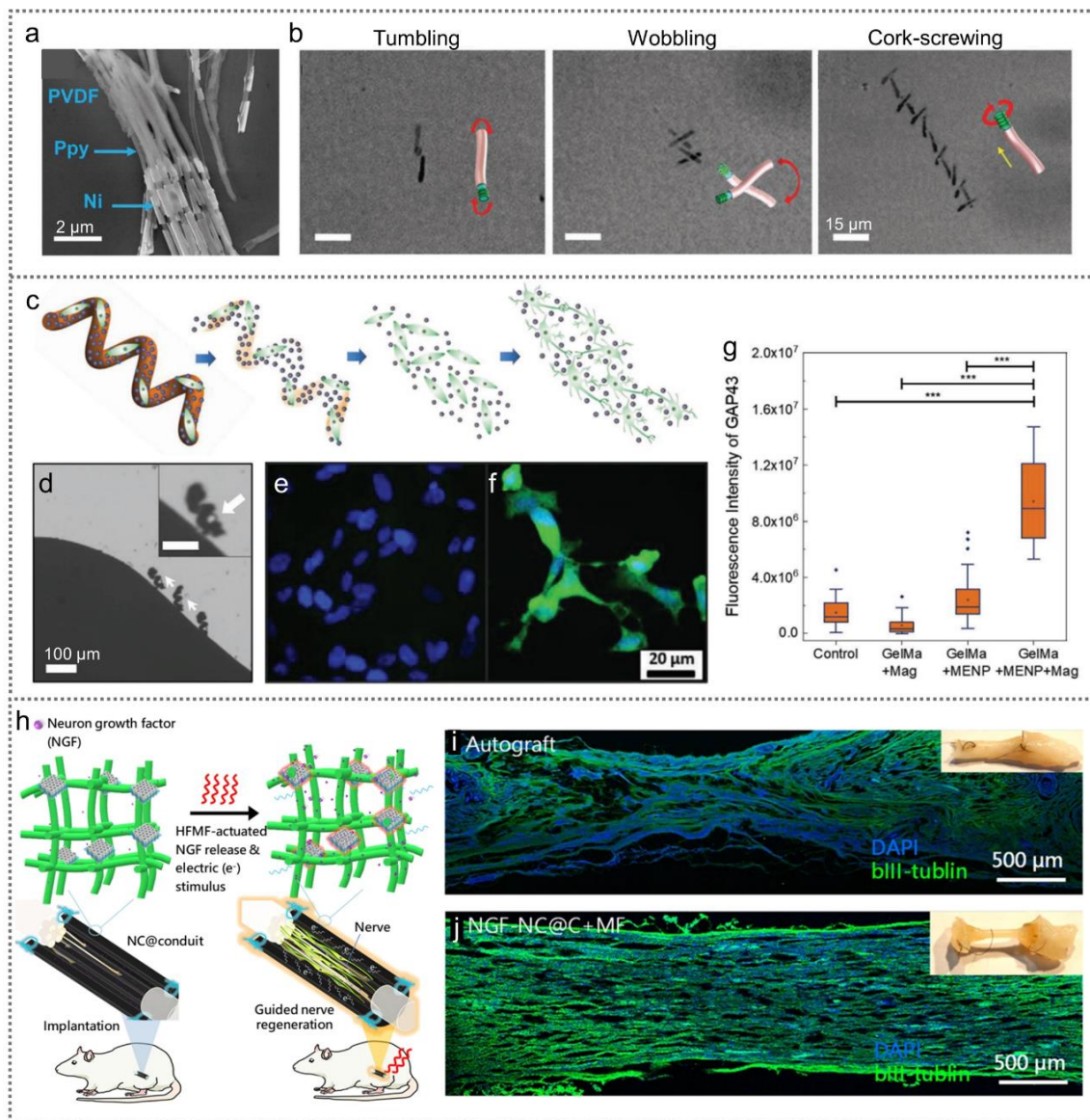


Figure 9. Magnetic field-driven PENGs for cell modulation: (a) a SEM image showing the hybrid nanoeels; (b) a time-lapse image showing the swimming behavior of the hybrid nanoeels, including tumbling, wobbling and corkscrewing. Reprinted with permission from ref. [83], Copyright 2019, WILEY-VCH. (c) A schematic diagram of the degradation process of the soft microswimmers and the neuronal differentiation of SH-SY5Y cells under a magnetic field; (d) a microswimmer loaded with cells driven by a rotating magnetic field. Fluorescent images of the cells on the (e) control and (f) soft microswimmers under magnetic stimulation. The nuclei are stained in blue and the neuronal specific protein GAP43 in green. (g) Box-and-whisker plots of the fluorescent intensities representing the level of GAP 43 expressed in SH-SY5Y cells (***p* < 0.001). Reprinted with permission from ref. [84], Copyright 2020, WILEY-VCH. (h) NC@C under magnetic field treatment promoting magneto-electric conversion into release growth factor and inducing neuron cell differentiation. Sciatic nerve defects harvested from (i) autograft and (j) NGF-NC@C+ magnetic field. Reprinted with permission from ref. [85], Copyright 2020, Springer Nature.

3.3.3. Cell Traction-Driven PENGs for Cell Modulation

There are abundant mechanical forces in cell activities, such as cell spreading, migration, contraction and cardiomyocyte beating. Thus, within the cellular microenvironment, cells continuously exert mechanical forces on the extracellular matrix (ECM). Similarly, the cells can also exert mechanical forces on the piezoelectric biomaterials. Murillo

et al. demonstrated that the electromechanical interaction between living cells and a ZnO nanosheet-based PENG induced a local electric field that could modulate cell activity, such as stimulating the cell motility and activating the calcium channels to induce intracellular calcium transients, depending on the cell type (Figure 10a,d) [89]. The effective piezoelectric coefficient of the ZnO nanosheets was 4–6 pm V⁻¹, according to a piezoresponse atomic force microscope. Under the weak force of cells (0.1–10 nN), ZnO nanosheets could generate a piezopotential in the range of 0.5–50 mV. The number of macrophages grown on ZnO nanosheets with a traveling distance exceeding 150 μm was twice of that grown on the control substrate, indicating that the electromechanical interaction of the ZnO nanosheet-based PENG increased the motility of macrophages and facilitated long-distance displacement (Figure 10c). In addition, 64% of the SaOS-2 cells grown on the ZnO nanosheets presented increases in [Ca²⁺]_i. By contrast, only 6% of the cells grown on glass coverslips showed increases in [Ca²⁺]_i, with low amplitudes of Ca²⁺ transients (Figure 10d). These results indicate that the cell adhesion forces could bend the ZnO nanosheets and induce a local electric field to stimulate the cells and alter their activities. Zhang et al. designed a piezoelectric PVDF with a nanostripe array structure for the neuron-like differentiation of mesenchymal stem cells (MSCs) [90]. The traction force of the living cells on the surface of the nanostriped PVDF could cause the deformation of the PVDF stripes, thereby generating a local piezopotential to provide continuous electrical stimulation to the living cells. According to the simulation, there was a piezopotential from 34 μV to 3.4 mV when cell traction forces increased from 0.1 to 10 nN (Figure 10e,f). However, the piezopotential induced by the cell force (10 nN) on flat PVDF film was only 960 nV, which was insignificant for the physiological activities of the cells. Thus, the nanotopography of the PVDF film could increase the generated piezopotential in response to cell migration and traction and it provided a stronger signal to stimulate the differentiation of the stem cells. Unlike the spindle-shaped and flat cell morphology in the control group, the MSCs on the nanostriped PVDF formed a neuron-like morphology, including highly refracted cell bodies and elongated nanostriped PVDF. Moreover, the mRNA and protein expression levels of neuronal marker Tuj-1 were significantly increased, indicating that the generated piezopotential of the nanostriped PVDF had a positive effect on the neuron-like differentiation of MSCs (Figure 10g). Inspired by the biophysical cues of ECM, Li et al. developed an electromechanical coupling 3D bio-nanogenerator composed of GO/PEDOT/Fe₃O₄/PAN fibers (GO, graphene oxide; PEDOT, poly(3,4-ethylenedioxythiophene); PAN, polyacrylonitrile), in which piezoelectric PAN was used as the electromechanical conversion unit [91]. The unique 3D structure of the bio-nanogenerator provided an ECM-like microenvironment for cell growth. It could also generate piezopotential up to millivolts through cell inherent force, thereby providing in situ electrostimulation for the adherent cells. Liu et al. prepared nanofibers with a suitable stiffness that was analogous to that of collagen using electrospinning technology [92]. Interestingly, the obvious mechanical deformation of the nanofibers was only observed after cell adhesion and mature focal adhesion formation (Figure 10h,i). Based on these dynamic mechanical forces in the cell microenvironment, a smart piezoelectric PVDF scaffold was designed that could generate piezopotential by cell traction force after cell adhesion, activate the transmembrane calcium channels for extracellular Ca²⁺ influx and promote the neuron-like differentiation of stem cells (Figure 10j,k). Since the deformation of the piezoelectric PVDF scaffold only occurred after cell adhesion, the on-demand electrical stimulation was only realized in the differentiation stage, thereby avoiding the inhibitory effect of early electrical stimulation on cell adhesion and spreading. In addition, Liu et al. designed a biodegradable piezoelectric PLLA that could generate piezopotential under joint load. This batteryless electrostimulation could promote protein adsorption and cell migration or recruitment, as well as induce endogenous TGF-β, thereby improving cartilage formation and cartilage regeneration. Rabbits with severe osteochondral defects regenerated hyaline cartilage and achieved complete cartilage healing after 1 to 2 months of self-driven electrical stimulation therapy [93]. This in situ electrical stimulation based on PENGs paves the way for smart scaffold design and future bioelectronic therapies.

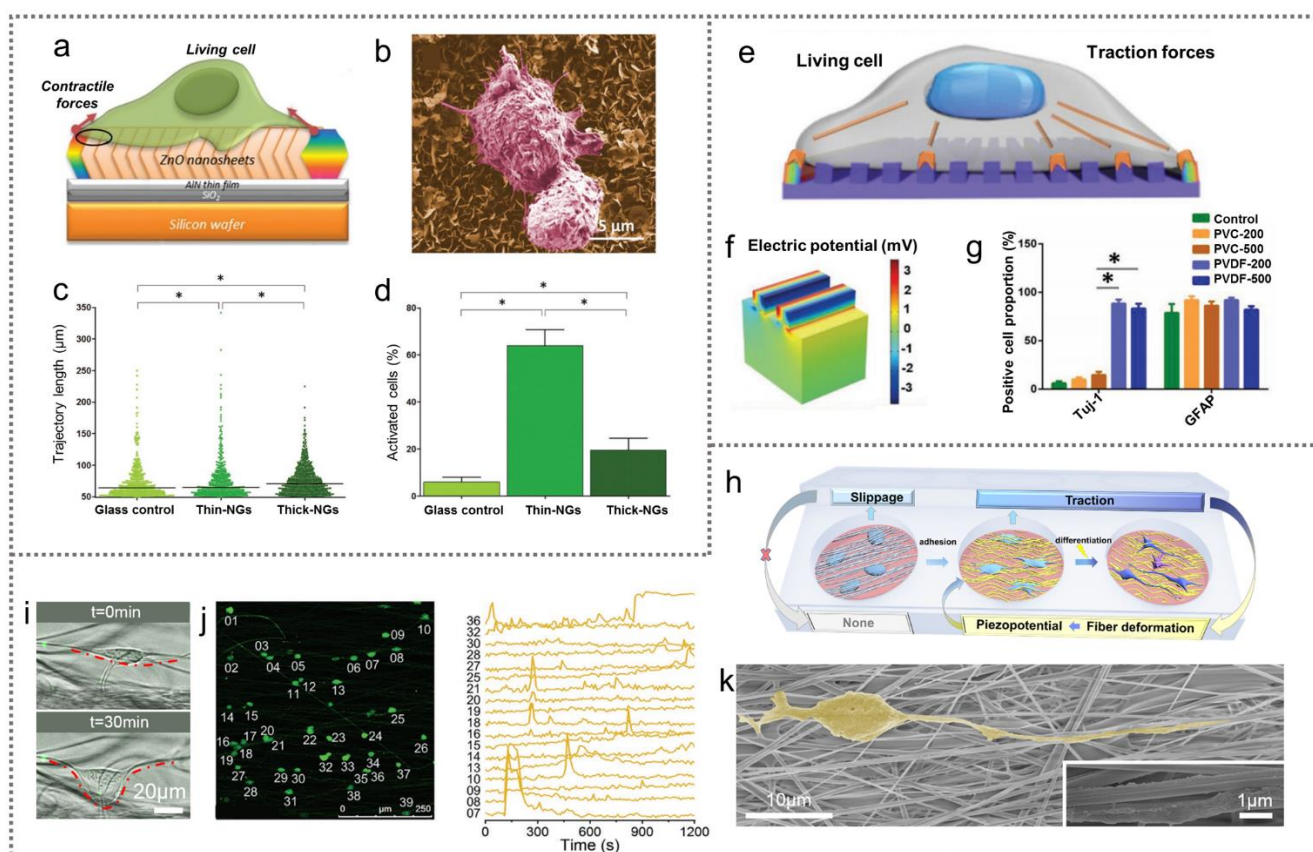


Figure 10. Cell traction-driven PENGs for cell modulation: (a) cell forces could bend the ZnO nanosheets of the PENG; (b) the micromorphology of the cells on the nanosheets; (c) the length of the trajectory represented the macrophage movement; (d) the quantification of activated Saos-2 cells with intracellular Ca^{2+} concentration change (* $p < 0.05$). Reprinted with permission from ref. [89], Copyright 2017, WILEY-VCH. (e) Cells grown on the nanostructured PVDF; (f) a simulation of the nanostructured PVDF generating a piezopotential of 3.4 mV when strained by a tangential force of 10 nN; (g) the percentage of Tuj-1 positive cells and GFAP positive cells (* $p < 0.05$). Reprinted with permission from ref. [90], Copyright 2019, WILEY-VCH. (h) A schematic diagram of the cell traction triggered, on-demand electrostimulation for neuron-like differentiation; (i) cell traction caused deformation along the nanofiber; (j) the cells grown on PVDF nanofibers with obvious transient calcium activity; (k) the morphology of the cells grown on the PVDF after differentiation. Reprinted with permission from ref. [92], Copyright 2021, WILEY-VCH.

4. Summary and Perspectives

In summary, EMNGs have shown promising applications in self-powered cell modulation, with impressive progress ranging from promoting cell migration, orientation and proliferation to regulating cell adhesion and differentiation (Table 1). Due to the advantages of convenience, good biosafety and patient compliance, EMNGs provide a promising approach for the clinical transformation of electrical stimulation. Generally, TENGs as an electrostimulation source need to cooperate with bioelectrodes to exert electrical stimulation to cells. By contrast, PENGs can achieve in situ wireless electrical stimulation while simultaneously acting as a biological scaffold. However, there are still great challenges and broad spaces for both basic research and clinic applications. Since the mechanical energy in the human body is weak and disordered, the structure of the nanogenerators needs to be reasonably designed and optimized to efficiently harvest the surrounding mechanical energy. Additionally, TENGs and PENGs can be hybridized with EMGs to combine the high voltage of the TENGs/PENGs and the high current of EMGs to realize multimodal electrostimulation, which is of great significance for broadening the application of EMNGs

in the biomedical field. At the same time, this combination also poses some challenges for EMNG technology, such as miniaturization, flexibility and system integration, etc. [14]. The long-term stability and safety of EMNGs in vivo still need to be verified. The current research is mainly focused on the effect of the open circuit voltage of the EMNG on the cells. In fact, the cell microenvironment is a complex electrophysiological environment. The voltage actually sensed by the cell depends not only on the output of the EMNG, but also on the electrical property of the culture medium and cell membrane [89]. Clarifying the actual voltage sensed by cells is more instructive for future research. In addition, the output of the EMNG is often a pulse wave, which is different from the square wave, sine wave and other waveforms produced by traditional electric stimulators. Thus, the electrostimulation conditions of the EMNG need to be further optimized and its underlying mechanism also needs to be explored. Additionally, the application of EMNGs can be extended to other electroactive cells, such as cardiomyocytes. The contractile force (20–140 nN) of cardiomyocytes is much higher than the cell traction force (1–10 nN) [90,94], which can be utilized to drive EMNGs more efficiently. Research at the cellular level is more conducive to revealing the regulatory mechanism of EMNG-based electrostimulation, with the ultimate goal of tissue function regulation and disease treatment. Both TENGs and PENGs have the advantages of small size, flexibility and good biocompatibility. To date, many wearable and implantable EMNGs have been reported that can efficiently harvest mechanical energy from living organisms, such as from joint motion, heartbeat and respiration, which have laid the foundation for further bioelectronic implants, especially for bones, hearts and muscles with abundant mechanical activities [93,95]. With the current progress and huge development space, EMNGs show tremendous potential for cell modulation and biomedical therapeutics.

Table 1. Electromechanical nanogenerators for cell modulation.

EMNG	Mode/Piezoelectric Scaffolds	Electrostimulation	Cells	Cell Modulation	Ref.
TENG	Implantable, contact-separation mode	10 V mm ⁻¹ , 1 Hz, 20 min/day, 5 days	Primary neurons	Cell alignment	[31]
	Contact-separation mode	30 μA, 3000 pulses/day, 21 days	MSCs	Neural differentiation	[35]
	Implantable, contact-separation mode	150 V cm ⁻¹ , 2 Hz, 1 h/day, 18 days	Preosteoblasts MC3T3-E1	Cell proliferation and osteogenic differentiation	[39]
	Contact-separation mode	12 V, 5–21 days	MC3T3-E1	Osteogenic differentiation	[40]
	Wearable, contact-separation mode	2 V cm ⁻¹ , 1 Hz, 6 h	Fibroblasts	Proliferation and differentiation into myofibroblasts	[43]
	Wearable, contact-separation mode	8 V, 1 Hz, 24 h	Fibroblasts	Cell alignment	[44]
	Implantable, contact-separation mode	100 mV mm ⁻¹ , 24 h	Fibroblasts	Cell migration	[33]
	Disk, freestanding mode	20 V, 20 Hz, 200 pluses	MCF-7, Hela, MSCs	Cell membrane permeability and drug delivery	[45]
	Contact-separation mode	20 V, 5 Hz, 200 pulses	MCF-7, MSCs	Cell membrane permeability and drug delivery	[28]
	Contact-separation mode	70 V, 4 kV cm ⁻¹	RBCs	Cell membrane permeability and drug release	[47]

Table 1. Cont.

EMNG	Mode/Piezoelectric Scaffolds	Electrostimulation	Cells	Cell Modulation	Ref.
PENG	Wearable, PVDF	20 μ A, 3 Hz, 2 h/day	MC3T3-E1	Cell proliferation and orientation and osteogenic differentiation	[67]
	PVDF-TrFE	$d_{31} = 16.17 \text{ pC N}^{-1}$ 6 mV, 6 nA,	Fibroblasts	Cell alignment and proliferation	[69]
	PVDF/BaTiO ₃	$d_{33} = 15.7 \text{ pC N}^{-1}$, −89.1 mV	MSCs	Regulate cell adhesion	[72]
	PVDF	$d_{33} = 16.22 \text{ pC N}^{-1}$	Macrophages	Proinflammatory macrophage polarization	[78]
	FeOOH/PVDF	$d_{33} = 27.2 \text{ pC N}^{-1}$	MSCs	Neural differentiation	[73]
	<i>S. platensis</i> @Fe ₃ O ₄ @BaTiO ₃	/	PC12 cells	Neural differentiation	[74]
	PVDF-TrFE/CoFe ₂ O ₄	/	PC12 cells	Neural differentiation	[75]
	Nylon-11	/	Dental pulp stem cells	Osteogenic differentiation	[77]
	CFO@BFO/GelMA	/	SHSY5Y cells	Neural differentiation	[84]
	NC@C	28–38 μ A	PC12	Neural differentiation	[85]
	ZnO nanosheets	300 μ V–45 mV	Macrophages	Stimulate the motility of macrophages	[89]
	PVDF	34 μ V–3.4 mV	MSCs	Neural differentiation	[90]
	GO/PEDOT/Fe ₃ O ₄ /PAN	$d_{33} = 4.5 \text{ pm V}^{-1}$, 14.1 μ V–1.41 mV	Hepatocytes and MSCs	Motility of primary hepatocytes and osteogenic differentiation of MSCs	[91]
	PVDF	$d_{33} = 24 \text{ pC N}^{-1}$, 0.73–133 mV	MSCs	Neural differentiation	[92]
PENG + TENG	Contact–separation mode PVDF/ZnO	1.5–2.7 V	Schwann cells	Cell proliferation and migration	[68]

Author Contributions: Conceptualization, L.L. and Z.L.; writing—original draft preparation, Z.L. and Z.W.; writing—review and editing, L.L.; supervision, L.L.; project administration, L.L.; funding acquisition, L.L. and Z.L. All authors have read and agreed to the published version of the manuscript.

Funding: The work was supported by the Strategic Priority Research Program of the Chinese Academy of Sciences (No. XDA16021100), the National Nature Science Foundation (No. 82072065, 81471784), the National Key R&D project from Minister of Science and Technology, China (2016YFA0202703), the National Youth Talent Support Program and the China Postdoctoral Science Foundation (No. BX2021299, 2021M703166).

Conflicts of Interest: The authors declare no conflict of interest.

References

- Liu, Z.R.; Wan, X.Y.; Wang, Z.L.; Li, L.L. Electroactive Biomaterials and Systems for Cell Fate Determination and Tissue Regeneration: Design and Applications. *Adv. Mater.* **2021**, *33*, 2007429. [[CrossRef](#)] [[PubMed](#)]
- da Silva, L.P.; Kundu, S.C.; Reis, R.L.; Correlo, V.M. Electric Phenomenon: A Disregarded Tool in Tissue Engineering and Regenerative Medicine. *Trends Biotechnol.* **2020**, *38*, 24–49. [[CrossRef](#)] [[PubMed](#)]
- Balint, R.; Cassidy, N.J.; Cartmell, S.H. Electrical Stimulation: A Novel Tool for Tissue Engineering. *Tissue Eng. Part B—Rev.* **2013**, *19*, 48–57. [[CrossRef](#)] [[PubMed](#)]
- Huang, G.; Li, F.; Zhao, X.; Ma, Y.; Li, Y.; Lin, M.; Jin, G.; Lu, T.J.; Genin, G.M.; Xu, F. Functional and Biomimetic Materials for Engineering of the Three-Dimensional Cell Microenvironment. *Chem. Rev.* **2017**, *117*, 12764–12850. [[CrossRef](#)]
- Jiang, D.; Shi, B.; Ouyang, H.; Fan, Y.; Wang, Z.L.; Li, Z. Emerging Implantable Energy Harvesters and Self-Powered Implantable Medical Electronics. *ACS Nano* **2020**, *14*, 6436–6448. [[CrossRef](#)]
- Zhu, B.; Luo, S.-C.; Zhao, H.; Lin, H.-A.; Sekine, J.; Nakao, A.; Chen, C.; Yamashita, Y.; Yu, H.-h. Large enhancement in neurite outgrowth on a cell membrane-mimicking conducting polymer. *Nat. Commun.* **2014**, *5*, 4523. [[CrossRef](#)]
- Zheng, Q.; Shi, B.; Li, Z.; Wang, Z.L. Recent Progress on Piezoelectric and Triboelectric Energy Harvesters in Biomedical Systems. *Adv. Sci.* **2017**, *4*, 1700029. [[CrossRef](#)]
- Jakešová, M.; Sjöström, T.A.; Đerek, V.; Poxson, D.; Berggren, M.; Głowacki, E.D.; Simon, D.T. Wireless organic electronic ion pumps driven by photovoltaics. *NPJ Flex. Electron.* **2019**, *3*, 14997. [[CrossRef](#)]

9. Ogawa, Y.; Kato, K.; Miyake, T.; Nagamine, K.; Ofuji, T.; Yoshino, S.; Nishizawa, M. Organic Transdermal Iontophoresis Patch with Built-in Biofuel Cell. *Adv. Health. Mater.* **2015**, *4*, 506–510. [[CrossRef](#)]
10. Xiao, X.X.; McGourty, K.D.; Magner, E. Enzymatic Biofuel Cells for Self-Powered, Controlled Drug Release. *J. Am. Chem. Soc.* **2020**, *142*, 11602–11609. [[CrossRef](#)]
11. Sato, H.; Minamitani, Y.; Ohnishi, N.; Fujiwara, Y.; Katsukie, S. Development of a High-Frequency Burst Pulse Generator for Cancer Cell Treatment and Comparison Between a High-Power Burst Pulse and a Single Pulse. *IEEE Trans. Plasma Sci.* **2020**, *48*, 1051–1059. [[CrossRef](#)]
12. Brezar, S.K.; Kranjc, M.; Cemazar, M.; Bucek, S.; Sersa, G.; Miklavcic, D. Electrotransfer of siRNA to Silence Enhanced Green Fluorescent Protein in Tumor Mediated by a High Intensity Pulsed Electromagnetic Field. *Vaccines* **2020**, *8*, 49. [[CrossRef](#)]
13. Novickij, V.; Kranjc, M.; Staigvila, G.; Dermol-Cerne, J.; Melesko, J.; Novickij, J.; Miklaveic, D. High-Pulsed Electromagnetic Field Generator for Contactless Permeabilization of Cells In Vitro. *IEEE Trans. Magn.* **2020**, *56*, 5000106. [[CrossRef](#)]
14. Vidal, J.V.; Slabov, V.; Kholkin, A.L.; dos Santos, M.P.S. Hybrid Triboelectric-Electromagnetic Nanogenerators for Mechanical Energy Harvesting: A Review. *Nano-Micro Lett.* **2021**, *13*, 199. [[CrossRef](#)]
15. Fan, F.R.; Tian, Z.Q.; Wang, Z.L. Flexible triboelectric generator! *Nano Energy* **2012**, *1*, 328–334. [[CrossRef](#)]
16. Liang, X.; Liu, Z.R.; Feng, Y.W.; Han, J.J.; Li, L.L.; An, J.; Chen, P.F.; Jiang, T.; Wang, Z.L. Spherical triboelectric nanogenerator based on spring-assisted swing structure for effective water wave energy harvesting. *Nano Energy* **2021**, *83*, 105836. [[CrossRef](#)]
17. Ren, Z.W.; Wang, Z.M.; Liu, Z.R.; Wang, L.F.; Guo, H.Y.; Li, L.L.; Li, S.T.; Chen, X.Y.; Tang, W.; Wang, Z.L. Energy Harvesting from Breeze Wind (0.7–6 m s⁻¹) Using Ultra-Stretchable Triboelectric Nanogenerator. *Adv. Energy Mater.* **2020**, *10*, 2001770. [[CrossRef](#)]
18. Yang, Y.; Wang, Z.L. Emerging nanogenerators: Powering the Internet of Things by high entropy energy. *iScience* **2021**, *24*, 102358. [[CrossRef](#)]
19. Luo, J.J.; Gao, W.C.; Wang, Z.L. The Triboelectric Nanogenerator as an Innovative Technology toward Intelligent Sports. *Adv. Mater.* **2021**, *33*, 2004178. [[CrossRef](#)]
20. Zhao, G.R.; Zhang, Y.W.; Shi, N.; Liu, Z.R.; Zhang, X.D.; Wu, M.Q.; Pan, C.F.; Liu, H.L.; Li, L.L.; Wang, Z.L. Transparent and stretchable triboelectric nanogenerator for self-powered tactile sensing. *Nano Energy* **2019**, *59*, 302–310. [[CrossRef](#)]
21. Nie, J.H.; Chen, X.Y.; Wang, Z.L. Electrically Responsive Materials and Devices Directly Driven by the High Voltage of Triboelectric Nanogenerators. *Adv. Funct. Mater.* **2019**, *29*, 1806351. [[CrossRef](#)]
22. Long, Y.; Li, J.; Yang, F.; Wang, J.Y.; Wang, X.D. Wearable and Implantable Electroceuticals for Therapeutic Electrostimulations. *Adv. Sci.* **2021**, *8*, 2004023. [[CrossRef](#)]
23. Wang, Y.; Wu, H.T.; Xu, L.; Zhang, H.N.; Yang, Y.; Wang, Z.L. Hierarchically patterned self-powered sensors for multifunctional tactile sensing. *Sci. Adv.* **2020**, *6*, eabb9083. [[CrossRef](#)]
24. Peng, X.; Dong, K.; Ye, C.Y.; Jiang, Y.; Zhai, S.Y.; Cheng, R.W.; Liu, D.; Gao, X.P.; Wang, J.; Wang, Z.L. A breathable, biodegradable, antibacterial, and self-powered electronic skin based on all-nanofiber triboelectric nanogenerators. *Sci. Adv.* **2020**, *6*, eaba9624. [[CrossRef](#)]
25. Sun, M.J.; Li, Z.; Yang, C.Y.; Lv, Y.J.; Yuan, L.; Shang, C.X.; Liang, S.Y.; Guo, B.W.; Liu, Y.; Li, Z.; et al. Nanogenerator-based devices for biomedical applications. *Nano Energy* **2021**, *89*, 106461. [[CrossRef](#)]
26. Zou, H.Y.; Zhang, Y.; Guo, L.T.; Wang, P.H.; He, X.; Dai, G.Z.; Zheng, H.W.; Chen, C.Y.; Wang, A.C.; Xu, C.; et al. Quantifying the triboelectric series. *Nat. Commun.* **2019**, *10*, 1427. [[CrossRef](#)]
27. Zou, H.Y.; Guo, L.T.; Xue, H.; Zhang, Y.; Shen, X.F.; Liu, X.T.; Wang, P.H.; He, X.; Dai, G.Z.; Jiang, P.; et al. Quantifying and understanding the triboelectric series of inorganic non-metallic materials. *Nat. Commun.* **2020**, *11*, 2093. [[CrossRef](#)]
28. Liu, Z.R.; Liang, X.; Liu, H.H.; Wang, Z.; Jiang, T.; Cheng, Y.Y.; Wu, M.Q.; Xiang, D.L.; Li, Z.; Wang, Z.L.; et al. High-Throughput and Self-Powered Electroporation System for Drug Delivery Assisted by Microfoam Electrode. *ACS Nano* **2020**, *14*, 15458–15467. [[CrossRef](#)]
29. Liang, X.; Jiang, T.; Liu, G.X.; Feng, Y.W.; Zhang, C.; Wang, Z.L. Spherical triboelectric nanogenerator integrated with power management module for harvesting multidirectional water wave energy. *Energy Environ. Sci.* **2020**, *13*, 277–285. [[CrossRef](#)]
30. Zhang, Z.C.; Yan, Q.Y.; Liu, Z.R.; Zhao, X.Y.; Wang, Z.; Sun, J.; Wang, Z.L.; Wang, R.R.; Li, L.L. Flexible MXene composed triboelectric nanogenerator via facile vacuum-assisted filtration method for self-powered biomechanical sensing. *Nano Energy* **2021**, *88*, 106257. [[CrossRef](#)]
31. Zheng, Q.; Zou, Y.; Zhang, Y.L.; Liu, Z.; Shi, B.J.; Wang, X.X.; Jin, Y.M.; Ouyang, H.; Li, Z.; Wang, Z.L. Biodegradable triboelectric nanogenerator as a life-time designed implantable power source. *Sci. Adv.* **2016**, *2*, e1501478. [[CrossRef](#)] [[PubMed](#)]
32. Jiang, W.; Li, H.; Liu, Z.; Li, Z.; Tian, J.; Shi, B.; Zou, Y.; Ouyang, H.; Zhao, C.; Zhao, L.; et al. Fully Bioabsorbable Natural-Materials-Based Triboelectric Nanogenerators. *Adv. Mater.* **2018**, *30*, 1801895. [[CrossRef](#)] [[PubMed](#)]
33. Li, Z.; Feng, H.Q.; Zheng, Q.; Li, H.; Zhao, C.C.; Ouyang, H.; Noreen, S.; Yu, M.; Su, F.; Liu, R.P.; et al. Photothermally tunable biodegradation of implantable triboelectric nanogenerators for tissue repairing. *Nano Energy* **2018**, *54*, 390–399. [[CrossRef](#)]
34. Wang, Z.L. Triboelectric Nanogenerator (TEENG)-Sparking an Energy and Sensor Revolution. *Adv. Energy Mater.* **2020**, *10*, 2000137. [[CrossRef](#)]
35. Guo, W.B.; Zhang, X.D.; Yu, X.; Wang, S.; Qiu, J.C.; Tang, W.; Li, L.L.; Liu, H.; Wang, Z.L. Self-Powered Electrical Stimulation for Enhancing Neural Differentiation of Mesenchymal Stem Cells on Graphene-Poly(3,4-ethylenedioxythiophene) Hybrid Microfibers. *ACS Nano* **2016**, *10*, 5086–5095. [[CrossRef](#)]
36. Pate, F.D. Bone chemistry and paleodiet. *J. Archaeol. Method Theory* **1994**, *1*, 161–209. [[CrossRef](#)]

37. Kumar, A.; Nune, K.C.; Misra, R.D.K. Electric field-mediated growth of osteoblasts—The significant impact of dynamic flow of medium. *Biomater. Sci.* **2016**, *4*, 136–144. [[CrossRef](#)]
38. Creecy, C.M.; O'Neill, C.F.; Arulanandam, B.P.; Sylvia, V.L.; Navara, C.S.; Bizios, R. Mesenchymal Stem Cell Osteodifferentiation in Response to Alternating Electric Current. *Tissue Eng. Part A* **2013**, *19*, 467–474. [[CrossRef](#)]
39. Tian, J.J.; Shi, R.; Liu, Z.; Ouyang, H.; Yu, M.; Zhao, C.C.; Zou, Y.; Jiang, D.J.; Zhang, J.S.; Li, Z. Self-powered implantable electrical stimulator for osteoblasts' proliferation and differentiation. *Nano Energy* **2019**, *59*, 705–714. [[CrossRef](#)]
40. Shi, R.; Zhang, J.S.; Tian, J.J.; Zhao, C.C.; Li, Z.; Zhang, Y.Z.; Li, Y.S.; Wu, C.G.; Tian, W.; Li, Z. An effective self-powered strategy to endow titanium implant surface with associated activity of anti-biofilm and osteogenesis. *Nano Energy* **2020**, *77*, 105201. [[CrossRef](#)]
41. Yao, G.; Kang, L.; Li, C.C.; Chen, S.H.; Wang, Q.; Yang, J.Z.; Long, Y.; Li, J.; Zhao, K.N.; Xu, W.N.; et al. A self-powered implantable and bioresorbable electrostimulation device for biofeedback bone fracture healing. *Proc. Natl. Acad. Sci. USA* **2021**, *118*, e2100772118. [[CrossRef](#)]
42. Nuccitelli, R. A role for endogenous electric fields in wound healing. *Curr. Top. Dev. Biol.* **2003**, *58*, 1–26.
43. Long, Y.; Wei, H.; Li, J.; Yao, G.; Yu, B.; Ni, D.L.; Gibson, A.L.F.; Lan, X.L.; Jiang, Y.D.; Cai, W.B.; et al. Effective Wound Healing Enabled by Discrete Alternative Electric Fields from Wearable Nanogenerators. *ACS Nano* **2018**, *12*, 12533–12540. [[CrossRef](#)]
44. Liu, A.P.; Long, Y.; Li, J.; Gu, L.; Karim, A.; Wang, X.D.; Gibson, A.L.F. Accelerated complete human skin architecture restoration after wounding by nanogenerator-driven electrostimulation. *J. Nanobiotechnol.* **2021**, *19*, 280. [[CrossRef](#)]
45. Liu, Z.R.; Nie, J.H.; Miao, B.; Li, J.D.; Cui, Y.B.; Wang, S.; Zhang, X.D.; Zhao, G.R.; Deng, Y.B.; Wu, Y.H.; et al. Self-Powered Intracellular Drug Delivery by a Biomechanical Energy-Driven Triboelectric Nanogenerator. *Adv. Mater.* **2019**, *31*, 1807795. [[CrossRef](#)]
46. Yang, C.B.; Yang, G.; Ouyang, Q.L.; Kuang, S.Y.; Song, P.Y.; Xu, G.X.; Poenar, D.P.; Zhu, G.; Yong, K.T.; Wang, Z.L. Nanowire-array-based gene electro-transfection system driven by human-motion operated triboelectric nanogenerator. *Nano Energy* **2019**, *64*, 103901. [[CrossRef](#)]
47. Zhao, C.C.; Feng, H.Q.; Zhang, L.J.; Li, Z.; Zou, Y.; Tan, P.C.; Ouyang, H.; Jiang, D.J.; Yu, M.; Wang, C.; et al. Highly Efficient In Vivo Cancer Therapy by an Implantable Magnet Triboelectric Nanogenerator. *Adv. Funct. Mater.* **2019**, *29*, 1808640. [[CrossRef](#)]
48. Ouyang, H.; Liu, Z.; Li, N.; Shi, B.J.; Zou, Y.; Xie, F.; Ma, Y.; Li, Z.; Li, H.; Zheng, Q.; et al. Symbiotic cardiac pacemaker. *Nat. Commun.* **2019**, *10*, 1821. [[CrossRef](#)]
49. Liu, Z.R.; Yu, X.; Li, L.L. Piezopotential augmented photo- and photoelectro-catalysis with a built-in electric field. *Chin. J. Catal.* **2020**, *41*, 534–549. [[CrossRef](#)]
50. Wang, Z.L. Progress in Piezotronics and Piezo-Phototronics. *Adv. Mater.* **2012**, *24*, 4632–4646. [[CrossRef](#)]
51. Gao, Z.; Zhou, J.; Gu, Y.; Fei, P.; Hao, Y.; Bao, G.; Wang, Z.L. Effects of piezoelectric potential on the transport characteristics of metal-ZnO nanowire-metal field effect transistor. *J. Appl. Phys.* **2009**, *105*, 113707. [[CrossRef](#)]
52. Shao, H.; Fang, J.; Wang, H.; Lang, C.; Lin, T. Robust Mechanical-to-Electrical Energy Conversion from Short-Distance Electrospun Poly(vinylidene fluoride) Fiber Webs. *ACS Appl. Mater. Interfaces* **2015**, *7*, 22551–22557. [[CrossRef](#)]
53. Yu, H.; Huang, T.; Lu, M.X.; Mao, M.Y.; Zhang, Q.H.; Wang, H.Z. Enhanced power output of an electrospun PVDF/MWCNTs-based nanogenerator by tuning its conductivity. *Nanotechnology* **2013**, *24*, 405401. [[CrossRef](#)]
54. Kapat, K.; Shubhra, Q.T.H.; Zhou, M.; Leeuwenburgh, S. Piezoelectric Nano-Biomaterials for Biomedicine and Tissue Regeneration. *Adv. Funct. Mater.* **2020**, *30*, 1909045. [[CrossRef](#)]
55. Chorsi, M.T.; Curry, E.J.; Chorsi, H.T.; Das, R.; Baroody, J.; Purohit, P.K.; Ilies, H.; Nguyen, T.D. Piezoelectric Biomaterials for Sensors and Actuators. *Adv. Mater.* **2019**, *31*, 1802084. [[CrossRef](#)]
56. Wang, Z.L.; Song, J.H. Piezoelectric nanogenerators based on zinc oxide nanowire arrays. *Science* **2006**, *312*, 242–246. [[CrossRef](#)]
57. Li, Z.; Zhu, G.; Yang, R.; Wang, A.C.; Wang, Z.L. Muscle-Driven In Vivo Nanogenerator. *Adv. Mater.* **2010**, *22*, 2534–2537. [[CrossRef](#)]
58. Dagdeviren, C.; Yang, B.D.; Su, Y.; Tran, P.L.; Joe, P.; Anderson, E.; Xia, J.; Doraiswamy, V.; Dehdashti, B.; Feng, X.; et al. Conformal piezoelectric energy harvesting and storage from motions of the heart, lung, and diaphragm. *Proc. Natl. Acad. Sci. USA* **2014**, *111*, 1927–1932. [[CrossRef](#)]
59. Cheng, X.; Xue, X.; Ma, Y.; Han, M.; Zhang, W.; Xu, Z.; Zhang, H.; Zhang, H. Implantable and self-powered blood pressure monitoring based on a piezoelectric thinfilm: Simulated, in vitro and in vivo studies. *Nano Energy* **2016**, *22*, 453–460. [[CrossRef](#)]
60. Jeong, C.K.; Han, J.H.; Palneedi, H.; Park, H.; Hwang, G.-T.; Joung, B.; Kim, S.-G.; Shin, H.J.; Kang, I.-S.; Ryu, J.; et al. Comprehensive biocompatibility of nontoxic and high-output flexible energy harvester using lead-free piezoceramic thin film. *APL Mater.* **2017**, *5*, 074102. [[CrossRef](#)]
61. Kondapalli, H.; Alazzawi, Y.; Malinowski, M.; Timek, T.; Chakrabarty, S. Feasibility of Self-Powering and Energy Harvesting Using Cardiac Valvular Perturbations. *IEEE Trans. Biomed. Circuits Syst.* **2018**, *12*, 1392–1400. [[CrossRef](#)] [[PubMed](#)]
62. Kim, D.H.; Shin, H.J.; Lee, H.; Jeong, C.K.; Park, H.; Hwang, G.-T.; Lee, H.-Y.; Joe, D.J.; Han, J.H.; Lee, S.H.; et al. In Vivo Self-Powered Wireless Transmission Using Biocompatible Flexible Energy Harvesters. *Adv. Funct. Mater.* **2017**, *27*, 1700341. [[CrossRef](#)]
63. Zhai, W.C.; Zhu, L.P.; Berbille, A.; Wang, Z.L. Flexible and wearable piezoelectric nanogenerators based on P(VDF-TrFE)/SnS nanocomposite micropillar array. *J. Appl. Phys.* **2021**, *129*, 095501. [[CrossRef](#)]

64. Zhou, L.L.; Zhu, L.P.; Yang, T.; Hou, X.M.; Du, Z.T.; Cao, S.; Wang, H.L.; Chou, K.C.; Wang, Z.L. Ultra-Stable and Durable Piezoelectric Nanogenerator with All-Weather Service Capability Based on N Doped 4H-SiC Nanohole Arrays. *Nano-Micro Lett.* **2022**, *14*, 30. [[CrossRef](#)]
65. Dong, K.; Peng, X.; Wang, Z.L. Fiber/Fabric-Based Piezoelectric and Triboelectric Nanogenerators for Flexible/Stretchable and Wearable Electronics and Artificial Intelligence. *Adv. Mater.* **2020**, *32*, 1902549. [[CrossRef](#)]
66. Song, Y.H.; Shi, Z.Q.; Hu, G.H.; Xiong, C.X.; Isogai, A.; Yang, Q.L. Recent advances in cellulose-based piezoelectric and triboelectric nanogenerators for energy harvesting: A review. *J. Mater. Chem. A* **2021**, *9*, 1910–1937. [[CrossRef](#)]
67. Zhang, Y.Z.; Lingling, X.; Liu, Z.; Cui, X.; Xiang, Z.; Bai, J.Y.; Jiang, D.J.; Xue, J.T.; Wang, C.; Lin, Y.X.; et al. Self-powered pulsed direct current stimulation system for enhancing osteogenesis in MC3T3-E1. *Nano Energy* **2021**, *85*, 106009. [[CrossRef](#)]
68. Jin, F.; Li, T.; Yuan, T.; Du, L.J.; Lai, C.T.; Wu, Q.; Zhao, Y.; Sun, F.Y.; Gu, L.; Wang, T.; et al. Physiologically Self-Regulated, Fully Implantable, Battery-Free System for Peripheral Nerve Restoration. *Adv. Mater.* **2021**, *33*, 2104175. [[CrossRef](#)]
69. Wang, A.C.; Liu, Z.; Hu, M.; Wang, C.C.; Zhang, X.D.; Shi, B.J.; Fan, Y.B.; Cui, Y.G.; Li, Z.; Ren, K.L. Piezoelectric nanofibrous scaffolds as in vivo energy harvesters for modifying fibroblast alignment and proliferation in wound healing. *Nano Energy* **2018**, *43*, 63–71. [[CrossRef](#)]
70. Mitragotri, S. Innovation—Healing sound: The use of ultrasound in drug delivery and other therapeutic applications. *Nat. Rev. Drug Discov.* **2005**, *4*, 255–260. [[CrossRef](#)]
71. Pan, X.T.; Bai, L.X.; Wang, H.; Wu, Q.Y.; Wang, H.Y.; Liu, S.; Xu, B.L.; Shi, X.H.; Liu, H.Y. Metal-Organic-Framework-Derived Carbon Nanostructure Augmented Sonodynamic Cancer Therapy. *Adv. Mater.* **2018**, *30*, 1800180. [[CrossRef](#)]
72. Wan, X.Y.; Zhang, X.D.; Liu, Z.R.; Zhang, J.M.; Li, Z.; Wang, Z.L.; Li, L.L. Noninvasive manipulation of cell adhesion for cell harvesting with piezoelectric composite film. *Appl. Mater. Today* **2021**, *25*, 101218. [[CrossRef](#)]
73. Zhang, R.T.; Han, S.W.; Liang, L.L.; Chen, Y.K.; Sun, B.J.; Liang, N.; Feng, Z.C.; Zhou, H.X.; Sun, C.H.; Liu, H.; et al. Ultrasonic-driven electrical signal-iron ion synergistic stimulation based on piezotronics induced neural differentiation of mesenchymal stem cells on FeOOH/PVDF nanofibrous hybrid membrane. *Nano Energy* **2021**, *87*, 106192. [[CrossRef](#)]
74. Liu, L.; Chen, B.; Liu, K.; Gao, J.B.; Ye, Y.C.; Wang, Z.; Qin, N.; Wilson, D.A.; Tu, Y.F.; Peng, F. Wireless Manipulation of Magnetic/Piezoelectric Micromotors for Precise Neural Stem-Like Cell Stimulation. *Adv. Funct. Mater.* **2020**, *30*, 1910108. [[CrossRef](#)]
75. Chen, X.Z.; Liu, J.H.; Dong, M.; Muller, L.; Chatzipirpiridis, G.; Hu, C.Z.; Terzopoulou, A.; Torlakcik, H.; Wang, X.P.; Mushtaq, F.; et al. Magnetically driven piezoelectric soft microswimmers for neuron-like cell delivery and neuronal differentiation. *Mater. Horiz.* **2019**, *6*, 1512–1516. [[CrossRef](#)]
76. Marino, A.; Arai, S.; Hou, Y.Y.; Sinibaldi, E.; Pellegrino, M.; Chang, Y.T.; Mazzolai, B.; Mattoli, V.; Suzuki, M.; Ciofani, G. Piezoelectric Nanoparticle-Assisted Wireless Neuronal Stimulation. *ACS Nano* **2015**, *9*, 7678–7689. [[CrossRef](#)]
77. Ma, B.J.; Liu, F.; Li, Z.; Duan, J.Z.; Kong, Y.; Hao, M.; Ge, S.H.; Jiang, H.D.; Liu, H. Piezoelectric nylon-11 nanoparticles with ultrasound assistance for high-efficiency promotion of stem cell osteogenic differentiation. *J. Mater. Chem. B* **2019**, *7*, 1847–1854. [[CrossRef](#)]
78. Kong, Y.; Liu, F.; Ma, B.J.; Duan, J.Z.; Yuan, W.H.; Sang, Y.H.; Han, L.; Wang, S.H.; Liu, H. Wireless Localized Electrical Stimulation Generated by an Ultrasound-Driven Piezoelectric Discharge Regulates Proinflammatory Macrophage Polarization. *Adv. Sci.* **2021**, *8*, 2100962. [[CrossRef](#)]
79. Kopyl, S.; Surmenev, R.; Surmeneva, M.; Fetisov, Y.; Kholkin, A. Magnetolectric effect: Principles and applications in biology and medicine—A review. *Mater. Today Bio* **2021**, *12*, 100149. [[CrossRef](#)]
80. Liu, X.L.; Li, D.; Zhao, H.X.; Dong, X.W.; Long, L.S.; Zheng, L.S. Inorganic-Organic Hybrid Molecular Materials: From Multiferroic to Magnetolectric. *Adv. Mater.* **2021**, *33*, 2004542. [[CrossRef](#)]
81. Tokura, Y.; Kanazawa, N. Magnetic Skyrmion Materials. *Chem. Rev.* **2021**, *121*, 2857–2897. [[CrossRef](#)]
82. Nair, M.; Guduru, R.; Liang, P.; Hong, J.; Sagar, V.; Khizroev, S. Externally controlled on-demand release of anti-HIV drug using magneto-electric nanoparticles as carriers. *Nat. Commun.* **2013**, *4*, 1707. [[CrossRef](#)]
83. Mushtaq, F.; Torlakcik, H.; Hoop, M.; Jang, B.J.; Carlson, F.; Grunow, T.; Laubli, N.; Ferreira, A.; Chen, X.Z.; Nelson, B.J.; et al. Motile Piezoelectric Nano-eels for Targeted Drug Delivery. *Adv. Funct. Mater.* **2019**, *29*, 1808135. [[CrossRef](#)]
84. Dong, M.; Wang, X.P.; Chen, X.Z.; Mushtaq, F.; Deng, S.Y.; Zhu, C.H.; Torlakcik, H.; Terzopoulou, A.; Qin, X.H.; Xiao, X.Z.; et al. 3D-Printed Soft Magnetolectric Microswimmers for Delivery and Differentiation of Neuron-Like Cells. *Adv. Funct. Mater.* **2020**, *30*, 1910323. [[CrossRef](#)]
85. Fang, J.H.; Hsu, H.H.; Hsu, R.S.; Peng, C.K.; Lu, Y.J.; Chen, Y.Y.; Chen, S.Y.; Hu, S.H. 4D printing of stretchable nanocookie@conduit material hosting biocues and magnetolectric stimulation for neurite sprouting. *NPG Asia Mater.* **2020**, *12*, 61. [[CrossRef](#)]
86. Shuai, C.J.; Yang, W.J.; He, C.X.; Peng, S.P.; Gao, C.D.; Yang, Y.W.; Qi, F.W.; Feng, P. A magnetic micro-environment in scaffolds for stimulating bone regeneration. *Mater. Des.* **2020**, *185*, 108275. [[CrossRef](#)]
87. Kozielski, K.L.; Jahanshahi, A.; Gilbert, H.B.; Yu, Y.; Erin, O.; Francisco, D.; Alosaimi, F.; Temel, Y.; Sitti, M. Nonresonant powering of injectable nanoelectrodes enables wireless deep brain stimulation in freely moving mice. *Sci. Adv.* **2021**, *7*, eabc4189. [[CrossRef](#)]
88. Singer, A.; Dutta, S.; Lewis, E.; Chen, Z.Y.; Chen, J.C.; Verma, N.; Avants, B.; Feldman, A.K.; O'Malley, J.; Beierlein, M.; et al. Magnetolectric Materials for Miniature, Wireless Neural Stimulation at Therapeutic Frequencies. *Neuron* **2020**, *107*, 631–643. [[CrossRef](#)]

89. Murillo, G.; Blanquer, A.; Vargas-Estevez, C.; Barrios, L.; Ibanez, E.; Nogues, C.; Esteve, J. Electromechanical Nanogenerator-Cell Interaction Modulates Cell Activity. *Adv. Mater.* **2017**, *29*, 1605048. [[CrossRef](#)]
90. Zhang, X.D.; Cui, X.; Wang, D.C.; Wang, S.; Liu, Z.R.; Zhao, G.R.; Zhang, Y.; Li, Z.; Wang, Z.L.; Li, L.L. Piezoelectric Nanotopography Induced Neuron-Like Differentiation of Stem Cells. *Adv. Funct. Mater.* **2019**, *29*, 1900372. [[CrossRef](#)]
91. Li, T.; Shi, C.M.; Jin, F.; Yang, F.; Gu, L.; Wang, T.; Dong, W.; Feng, Z.Q. Cell activity modulation and its specific function maintenance by bioinspired electromechanical nanogenerator. *Sci. Adv.* **2021**, *7*, eabh2350. [[CrossRef](#)] [[PubMed](#)]
92. Liu, Z.R.; Cai, M.J.; Zhang, X.D.; Yu, X.; Wang, S.; Wan, X.Y.; Wang, Z.L.; Li, L.L. Cell-Traction-Triggered On-Demand Electrical Stimulation for Neuron-Like Differentiation. *Adv. Mater.* **2021**, *33*, 2106317. [[CrossRef](#)] [[PubMed](#)]
93. Liu, Y.; Dzidotor, G.; Le, T.T.; Vinikoor, T.; Morgan, K.; Curry, E.J.; Das, R.; McClinton, A.; Eisenberg, E.; Apuzzo, L.N.; et al. Exercise-induced piezoelectric stimulation for cartilage regeneration in rabbits. *Sci. Transl. Med.* **2022**, *14*, 627. [[CrossRef](#)]
94. You, J.; Moon, H.; Lee, B.Y.; Jin, J.Y.; Chang, Z.E.; Kim, S.Y.; Park, J.; Hwang, Y.S.; Kim, J. Cardiomyocyte sensor responsive to changes in physical and chemical environments. *J. Biomech.* **2014**, *47*, 400–409. [[CrossRef](#)] [[PubMed](#)]
95. Soares dos Santos, M.P.; Coutinho, J.; Marote, A.; Sousa, B.; Ramos, A.; Ferreira, J.A.F.; Bernardo, R.; Rodrigues, A.; Marques, A.T.; da Cruz e Silva, O.A.; et al. Capacitive technologies for highly controlled and personalized electrical stimulation by implantable biomedical systems. *Sci. Rep.* **2019**, *9*, 5001. [[CrossRef](#)] [[PubMed](#)]